AEAT-ESD-278

Durability and Lifetime Predictions of Adhesive Joints

Ambrose Taylor

December 1996

AEAT-ESD-278

Durability and Lifetime Predictions of Adhesive Joints

Ambrose Taylor

December 1996

Title	Durability and Lifetime Predictions of Adhesive Joints
Customer	
Customer reference	AH 9/3
Confidentiality, copyright and reproduction	Copyright AEA Technology plc 1996 All rights reserved. Enquiries about copyright and reproduction should be addressed to the Commerical Manager, AEA Technology plc.
File reference	29570 600
Reference number	AEAT-ESD-278

AEA Technology plc
424, Harwell
Didcot
Oxfordshire
OX11 0RA
Telephone 01235 432060
Facsimile 01235 432481

AEA Technology is the trading name of
AEA Technology plc

AEA Technology is certified to ISO9001

Report Manager	Name	J McCarthy
Approved by	Name	G C Eckold
	Signature	
	Date	

Contents

Foreword

Many UK manufacturers are aware of the merits of adhesives in certain critical roles. However, the range of applications of adhesives is still limited largely due to the lack of consistent test methods and validated test data which the engineer needs in order to specify adhesives for a given application. In a recent survey the Centre for Adhesive Technology was commissionined by the DTI to establish specific areas where validated test methods could improve confidence in predicting joint life. The survey identified measurement methods for use in design, environmental durability and process control as priority areas and five projects were finally selected by the DTI for support through the Measurement Technology and Standards (MTS) budget. The projects started in December 1992 and are 100% funded by the DTI at the level of £5.4M over three years.

A key area that was identified in the survey was the need to provide a means for the quantification and prediction of the lifetim of bonded joints when exposed to a hostile environment, and this forms the basis of Project 3 of the Adhesives programme. The project is being carried out through a collaboration of AEA Technology and Oxford Brookes University, together with important contributions from Imperial College, DRA (Holton Heath) and Loughborough University.

The basis of the project is that there still remains considerable uncertainty in predicting joint lifetime under typical operating conditions, despite the enormous prior investment in durability studies. This difficulty represents perhaps the single most significant impediment to the wider use of adhesive technology. The programme combines a fresh look at testing procedures and predictive methods with a rigorous examination of previous work. Together the two strands of the approach produce a work plan which has a strong industrial focus. In addition to tasks on test methods and design, a series of forensic studies will be undertaken on examples of bonded structures which have seen extensive service life, in order to evaluate the reasons for their success. This will provide practical feedback into the other aspects of the programme as well as indicating to designers tangible evidence of the potential of bonding technology which they will be able to relate to their own particular application.

This project is divided into seven tasks:

- *Appraisal of Test Methods and Durability Data*
- *Development of an Experimental Database*
- *Characterisationof the Moisture Absorption Process*
- *Forensic Studies*
- *Assessment of Microstructural Failure Mechanisms*
- *Develement of Methodologies for Life Prediction*
- *Technology Transfer*

1 Introduction

In recent years the use of adhesives has increased as manufacturers become aware of the advantages they can offer over conventional joining techniques. However to be confident in their use it is necessary to evaluate the performance of joints, especially as the strength of the joint tends to decrease with exposure to moisture or fatigue loading.

This work will investigate the effect of an aqueous environment on the fracture energy of two typical adhesive systems under cyclic loading (i.e. dynamic fatigue). An acrylic and an epoxy adhesive will be used to bond steel and aluminium substrates prepared with either a gritblast and degrease or a chromic-acid etch surface treatment.

The initial work will find the static fracture energy, G_C, of the adhesives. This will be followed by fatigue tests, to give the relationship between the rate of crack growth per cycle, da/dN, against the maximum strain energy release rate, G_{max}. These fatigue tests will be conducted in a 'dry' environment of 23±1°C and 55 % relative humidity, and a 'wet' environment of immersion in distilled water at 28±1°C. From this data it will be possible to determine whether a threshold strain energy release rate, G_{th}, exists, below which crack growth does not occur. These data will then be used to attempt to predict the life of single lap joints under fatigue in an aqueous environment.

2 BACKGROUND

2.1 INTRODUCTION

This work uses a linear-elastic fracture-mechanics (LEFM) approach to assess the effect of an environment on adhesive joints. This section provides a very brief introduction to the principles of fracture mechanics, and to the mechanisms of water attack on adhesive joints.

2.2 FRACTURE MECHANICS

The theoretical strength of a material, based on the molecular forces within it, is several orders of magnitude greater than that observed. The basic tenet of fracture mechanics is that intrinsic flaws are present in any material, which propagate and cause premature failure. Fracture mechanics aims to model this process, and allow the engineer to predict the observed strength.

Fracture is said to occur when sufficient energy is released by the growth of a crack to supply the energy requirements of the new surface formed. The energy required to extend a crack over a unit area, for a given material, is termed the fracture energy, G_C. The value of G_C is independent of the geometry of the body. Crack growth occurs when the strain energy release rate in the specimen is equal to G_C.

Loads may be applied to a crack in three modes. Tensile opening, mode I, is considered the most important as it is the most commonly seen, and the mode in which failure most often occurs. Thus the parameter of interest will be the mode I fracture energy.

The overall loading response of the specimen can be considered to be linear elastic providing any plasticity is localised to a small zone around the crack tip. The specimens used in this work meet the size conditions that allow the assumptions of LEFM to be made[1].

2.3 MECHANISMS OF ATTACK BY WATER

Water can affect the strength of adhesive joints, as reported by Comyn[2], by attacking the adhesive, the substrate, or the interface between them. It can reach these areas by diffusion through the adhesive or by transport along the interface[2-4], which will be discussed further in section 5.5.2. Some of the other processes, such as diffusion through the substrates, are not applicable here as the substrates are not porous.

The mechanisms by which the joint can be weakened can include:

Reversible alteration of adhesive properties, e.g. plasticisation.
Irreversible alteration of adhesive properties, e.g. hydrolysis or crazing.
Swelling stresses in adhesive.
Displacement of adhesive from interface.
Hydration and weakening of metal oxide at interface.

These mechanisms are mostly detrimental to joint durability, but some may be beneficial, for example plasticisation allows the adhesive to relax and may reduce the stress concentration at the crack tip.

3 Materials and Surface Treatments

3.1 ADHESIVES

The adhesives used were common to much of the MTS programme. These were a rubber-toughened epoxy, 'AV119' (from Ciba Polymers), and an acrylic, 'F241' (from Permabond), as detailed in Table 1.

3.2 SUBSTRATES

Mild steel and aluminium alloy substrates were used. The MTS programme specified grades EN32B and BS5251 respectively. However the aluminium was found to plastically deform, which violates the assumptions of LEFM, and so the BS5251 grade was replaced by the higher yield strength BS5083 alloy.

3.3 SURFACE TREATMENT

3.3.1 Introduction

Steel specimens were prepared with a gritblast and degrease surface treatment. A chromic-acid etch (CAE) or a gritblast and degrease (GB/DG) treatment was used for the aluminium alloy substrates. The CAE treatment is a surface treatment which has been shown to improve durability[5]. Further details of these treatments can be found in report number 3 of the MTS project 4[6]. Bonding was completed as soon as possible after surface preparation to reduce the risk of surface degradation or contamination.

3.3.2 Gritblast and Degrease

The adherends were wiped with acetone until the tissue used remained clean after each stroke, showing that no further contamination was being removed. They were then gritblasted with alumina grit at 60 or 80 psi for aluminium and steel respectively. The grit was sprayed at an angle of 45° to the surface so that the particles bounced off the surface rather than becoming embedded in it. The adherends were then degreased again by wiping with acetone as above.

3.3.3 Chromic-Acid Etch

The adherends were prepared as section 3.3.2 above, then placed in a bath of chromic-acid etch[6] at 68°C for 10 minutes. They were rinsed with tap water and placed in a bath of tap water for 15 minutes, before being rinsed with distilled water and dried in warm air.

Adhesive	Manufacturer	Form	Cure Temperature, °C	Cure Time	Tg, °C
'AV119'	Ciba Polymers	One part epoxy	120	60 min	113
'F241'	Permabond	Two part acrylic	23	24 hrs	-25

Table 1. Adhesives used in the current work, with cure conditions and glass transition temperature, T_g.

4 Static Tapered Double Cantilever Beam Tests

4.1 INTRODUCTION

As discussed earlier, the static fracture energy of a material can be found by performing a fracture test at a constant displacement rate. For this work the tapered double-cantilever beam (TDCB) geometry was used, as shown in Figure 1. This method has been well validated previously[7-10], and used to describe both static and fatigue crack propagation.

4.2 ANALYSIS

Williams[11] has shown that for a general linear elastic double cantilever beam, the energy release rate, G, is given by:

$$G = \frac{P^2}{2b}\frac{dC}{da} = \frac{P}{2b}\left(\frac{u}{C}\right)\frac{dC}{da} = \frac{1}{2b}\left(\frac{u}{C}\right)^2\frac{dC}{da} \qquad (1)$$

where P is the applied load, b is the width of the specimen, C is the compliance, a is the crack length, and u is the displacement.

The TDCB geometry is designed such that the value of dC/da is constant as the crack grows through the specimen[7]:

$$\frac{dC}{da} = \frac{8m_b}{E_s b} \qquad (2)$$

where E_S is the modulus of the substrate and:

$$m_b = \left(\frac{3a^2}{z^3} + \frac{1}{z}\right) = \text{Constant} \qquad (3)$$

where z is the height of the substrate, see Figure 1, and m_b = 2 mm^{-1}.

Substituting Equation 2 into Equation 1 gives:

$$G = \frac{P^2}{2b}\frac{8m_b}{E_s b} \qquad (4)$$

Note that the calculated value of G is independent of crack length with this geometry.

The adhesive fracture energy can be calculated from the crack propagation load, P_C.

$$G_C = \frac{4P_c^2 m_b}{E_s b^2} \qquad (5)$$

4.3 SPECIMEN MANUFACTURE

The steel and aluminium alloy substrates used were 10 mm thick. This is sufficient to fulfil the requirement for plane-strain conditions[1]. The tapered profile of the beams was milled on a computer numerically-controlled milling machine.

After surface preparation, see section 3.3, the adhesive was applied to both substrates. The 'AV119' adhesive was applied as a bead and spread with a spatula until the whole surface was

covered. Care was taken not to trap air bubbles. The 'F241' adhesive consisted of a resin and a liquid hardener (aniline). A thin layer of hardener was painted onto both surfaces, ensuring that the whole area was wetted. The resin was applied as a bead to both surfaces, but not spread (as per the manufacturer's instructions).

A piece of 0.4 mm diameter stainless steel wire was placed at either end of the joint to give a constant bondline thickness. A double thickness of aluminium foil coated with release agent was placed in the middle of the bondline as a starter crack to encourage cohesive-in-adhesive failure. The two halves of the beam were brought together in a jig shaped such that pressure is applied to three points along the length of the beam. The bolts securing the two platens of the jig were torqued to 5 Nm. The adhesive was then cured, see Table 1.

After curing most of the excess adhesive was carefully removed using a chisel, the remainder being sanded off. On one side of the specimen a 10 mm wide strip, running the length of the specimen and spanning the bondline, was spray-painted with a thin layer of white paint. This enabled the position of the crack tip to be seen more clearly during testing.

4.4 EXPERIMENTAL PROCEDURE

The TDCB specimens were tested on a screw-driven Instron testing machine at a constant crosshead speed of 0.5 or 1 mm/min. The force versus time response of the specimens was recorded. The crack length was measured optically at intervals using a travelling microscope, and marked on the force versus time chart.

4.5 RESULTS

Values of the fracture energy were calculated via Equation 5. Most specimens failed by stable crack growth at a constant load, and hence the calculated fracture energy is constant, see Figure 2. The results obtained for the adhesive/substrate combinations are shown in Table 2.

As G_C is considered to be a material property, it would be expected that its value would be independent of the substrate used if failure was purely cohesive-in-adhesive. This was found to be the case for the 'F241' adhesive with all three substrates, with G_C equal to 820 J/m^2, see Table 2.

The 'AV119'/steel specimens did not all exhibit the stable cohesive crack propagation seen in the 'F241' tests. Here two types of failure were observed. Firstly, where stable crack growth occurred, see Figure 2, the failure was apparently interfacial, and a G_C value of 400 J/m^2 was measured. Secondly, stick/slip propagation was also observed, see Figure 3. Here the crack propagated a short distance, typically between 80 and 100 mm, and arrested. The speed of crack propagation was much greater than the crosshead speed. The specimens failed by a series of these crack propagation and arrest events. Failure was cohesive-in-adhesive, with small areas of apparently interfacial failure at the crack arrest/propagation points, see Figure 4. Some steel specimens exhibited both types of failure. The G_C values obtained are shown in Table 2. Initiation and arrest values are shown where applicable. The GB/DG aluminium specimens also failed in a stick/slip manner.

The CAE treated 'AV119' specimens exhibited stable crack growth with a cohesive-in-adhesive locus of failure. The average value of G_C was 700 J/m^2.

The initial crack propagation was often from a somewhat higher load value, and hence at a higher fracture energy, than might be expected from the rest of the test, see Figure 2. This is because propagation is from the end of the foil insert, which is not as sharp as a natural crack, and thus does not give a true 'lower-bound' value. Such artificially high values were ignored.

4.6 CONCLUSIONS

The 'F241' adhesive gave a static fracture energy of 820 J/m^2 with all the substrates and surface treatments used. The static tests on the 'AV119' adhesive gave a G_C value of 700 J/m^2 on the CAE aluminium alloy substrates. Here failure was stable and cohesive within the adhesive. Apparently interfacial failure was sometimes observed with the 'AV119' adhesive on steel substrates, and this failure mode gave a G_C value of 400 J/m^2. Stick/slip failure was also observed for the 'AV119' adhesive on steel and GB/DG aluminium alloy substrates. These data are summarised in Table 2.

	Fracture Energy, G_C, J/m^2	**Standard Deviation, J/m^2**
CAE Aluminium	700	70
GB/DG Aluminium	520/205	70
GB/DG Steel	450 / 190	75

2(a) 'AV119' adhesive.

	Fracture Energy, G_C, J/m^2	**Standard Deviation, J/m^2**
CAE Aluminium	820	30
GB/DG Aluminium	820	40
GB/DG Steel	840	30

2(b) 'F241' adhesive.

Note Where two values are shown these represent the initiation and arrest values respectively for stick/slip crack propagation.

Table 2. Fracture energy values from static TDCB tests, (a) 'AV119' adhesive, (b) 'F241' adhesive.

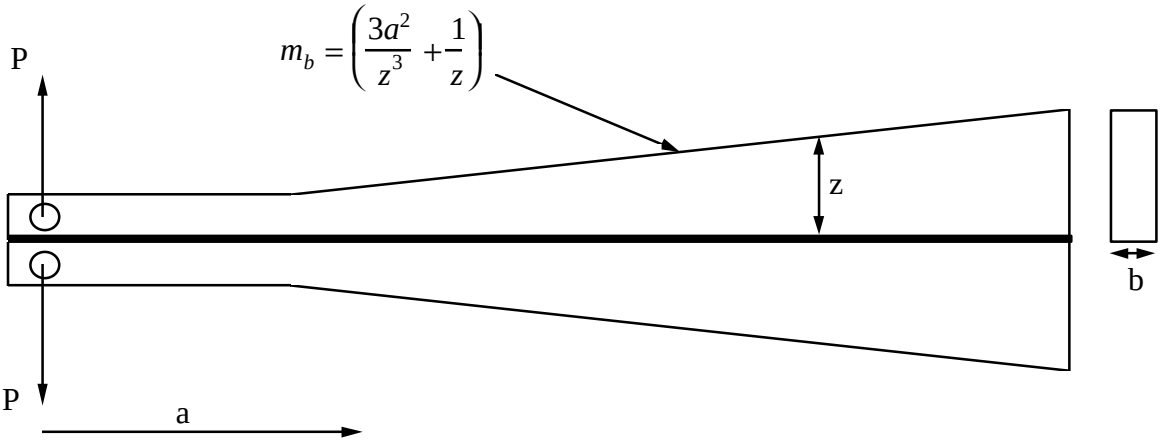

Figure 1. The tapered double cantilever beam (TDCB) specimen.

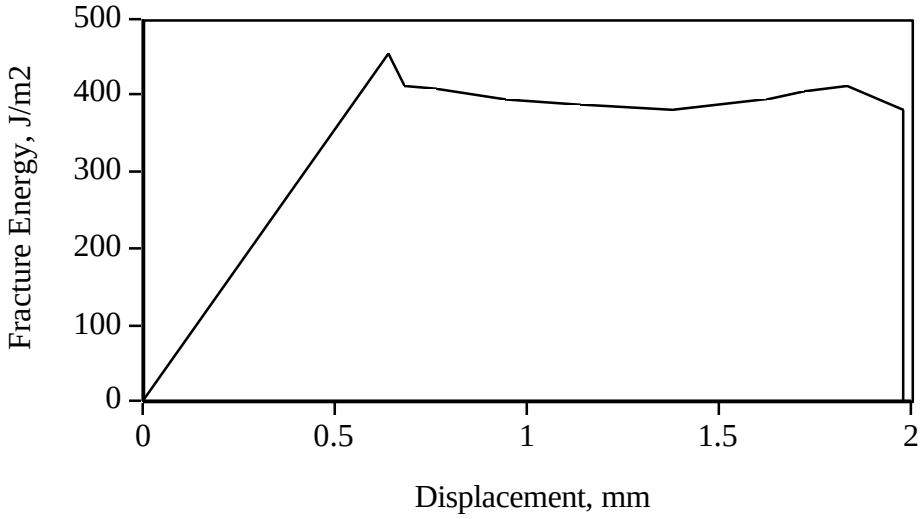

Figure 2. Fracture energy versus displacement for static 'AV119'/steel TDCB test, showing stable crack growth and a somewhat higher initiation value.

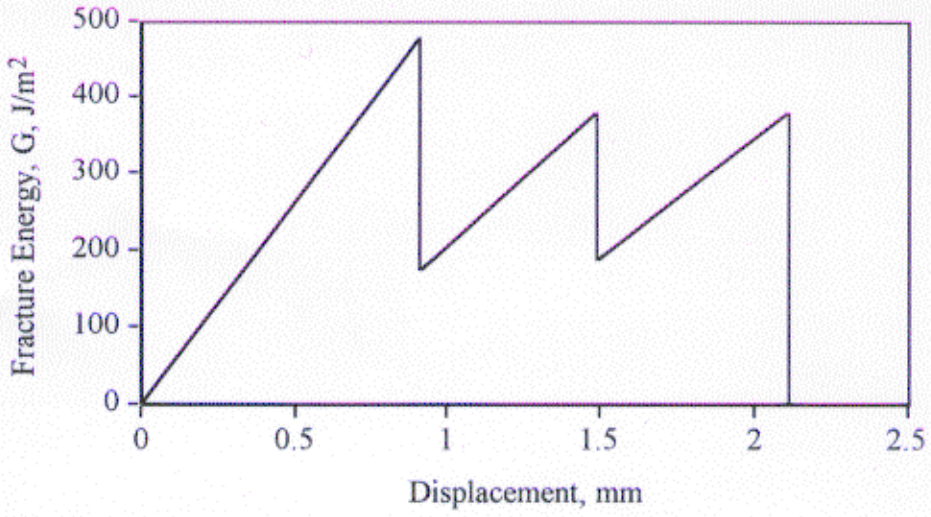

Figure 3. **Fracture energy versus displacement graph for static 'AV119'/steel TDCB test showing stick/slip crack growth.**

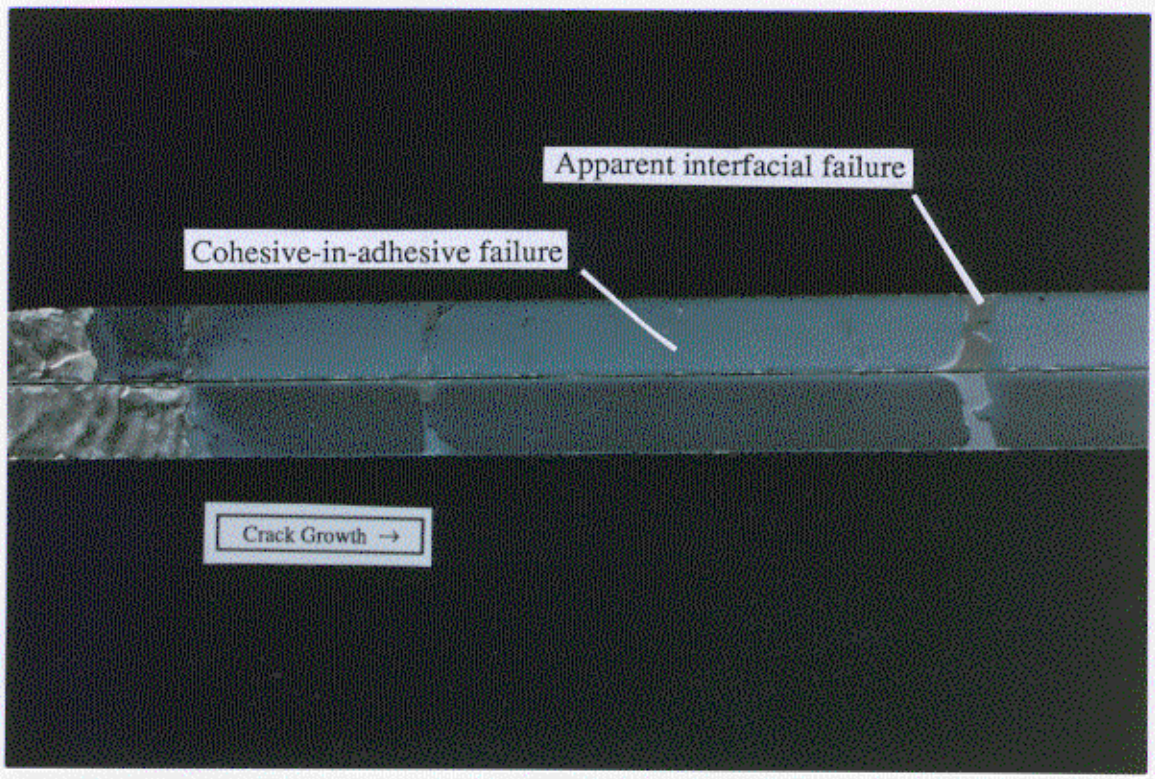

Figure 4. **Fracture surface of static 'AV119'/steel test specimen showing cohesive failure, plus areas of apparently interfacial failure between arrest and initiation points from stick/slip crack growth.**

5 Fatigue Tapered Double-Cantilever Beam Tests

5.1 INTRODUCTION

In cyclic fatigue tests, crack growth can occur at values of the strain energy release rate that are less than G_C. Here the maximum applied strain energy release rate is the controlling factor. The tests used the same TDCB geometry as the static testing. The joints were subjected to cyclic loading at 5 Hz. The rate of crack growth per cycle, da/dN, was measured as a function of the maximum strain energy release rate, G_{max}. Joints were tested 'dry', at 23°C and 55 % relative humidity, and immersed in water at 28°C.

5.2 ANALYSIS

As shown in section 4.2 above, the adhesive fracture energy can be calculated from static tests by:

$$G_C = \frac{4 P_c^2 m_b}{E_s b^2} \qquad (6)$$

Similarly in fatigue loading, the maximum strain energy release rate, G_{max}, can be found from:

$$G_{\max} = \frac{4 P_{\max}^2 m_b}{E_s b^2} \qquad (7)$$

The calculated value of G_{max} can be plotted against the rate of crack growth per cycle, da/dN, on logarithmic axes, see Figure 5. The central linear portion of the curve (II) can be described by a Paris Law relationship:

$$\frac{da}{dN} = D\left(G_{\max}\right)^n \qquad (8)$$

where D and n are found by fitting the relationship to the data and may be considered as material parameters.

It is also possible to use ΔG, the applied range of strain energy release rate, in place of G_{max}[8], where:

$$\Delta G = G_{\max} - G_{\min} \qquad (9)$$

This leads to a similar relationship with the rate of crack growth per cycle to that seen above:

$$\frac{da}{dN} = A_f (\Delta G)^q \qquad (10)$$

where A_f and q are constants.

However during the unloading part of the fatigue cycle the fracture surfaces can come into contact. This interference and the generation of debris on the surface may prevent the crack from closing, and hence produce a G_{min} value that is artificially high. Thus it has been suggested that the use of G_{max} is preferable[12,13].

Returning to Figure 5, the whole curve is of a sigmoidal form, and can be described by:

$$\frac{da}{dN} = DG_{max}^{n} \left\{ \frac{\left[1 - \left(\frac{G_{th}}{G_{max}}\right)^{n_1}\right]}{\left[1 - \left(\frac{G_{max}}{G_c}\right)^{n_2}\right]} \right\} \qquad (11)$$

where n_1, and n_2 are material parameters which are calculated by fitting Equation 11 to the experimental data, the values of D and n having been found from Equation 8. The threshold value, G_{th}, is the minimum value of the fracture energy (I) and G_C is the quasi-static value (III), as obtained in section 4. The threshold value, G_{th}, can be used as a very conservative design parameter, as below this value a crack will not propagate.

5.3 EXPERIMENTAL PROCEDURE

Specimens were prepared in the same way as for the static testing. 'Dry' tests were conducted at 23±1°C in about 55 % relative humidity. 'Wet' tests were performed in a tank of distilled water, kept at a constant temperature of 28±1°C using a water circulator/heater. Steel specimens for 'wet' testing were sprayed with paint to reduce corrosion, and hence discoloration of the water which would obscure the crack. The adhesive was left exposed (except for the thin layer of white paint on one side) so as not to effect the rate of water uptake.

The beams were tested at a frequency of 5 Hz using a servo-hydraulic machine, under displacement control. A sinusoidal waveform, with a constant displacement ratio ($\delta_{min}/\delta_{max}$) of 0.5 was used. The number of cycles, the maximum applied load, and the crack length were recorded at intervals. The crack length was monitored optically using a travelling microscope, and additionally for the 'dry' tests using a potential drop technique, as described below.

5.4 CRACK PROPAGATION GAUGES

5.4.1 Introduction

The crack growth in the 'dry' tests was monitored using a crack propagation gauge system with a potential drop technique. This uses the 'Fractomat' system from Rumul, Switzerland. A foil gauge is bonded to the side of the specimen, see Figure 6, through which a constant current is passed. As the crack grows the gauge breaks, increasing its resistance. The resultant change in potential (voltage) is converted to a crack length and logged at intervals on computer, see Figure 7.

5.4.2 Gauge Application

A line was scribed on the specimen about 100 mm from the loading point to locate the end of the gauge. Prior to bonding the specimen was degreased. The areas of the specimen where the gauge and the soldering terminals would be bonded were etched by wiping with a surface conditioner, followed by a neutraliser. The gauge was laid on a clean surface and picked up with pressure-sensitive tape. It was placed in position on the specimen using the alignment marks on the gauge to ensure it was central over the adhesive layer. The tape was secured at one end, and peeled back to expose the underside of the gauge. This process was repeated for the two pairs of soldering terminals. The adhesive used was a two part epoxy. This was mixed according to the manufacturer's instructions and applied to the gauge and the relevant areas of the specimen. The gauge and terminals were smoothed onto the surface of the specimen. The pressure-sensitive tape holds the gauge in position until the adhesive cures. A strip of PTFE was placed over the specimen, and covered with a sheet of silicone rubber and a metal backing plate. Pressure was applied using two spring clamps. The adhesive was cured for 2 hours at 70°C. After curing the pressure-sensitive tape was removed, and wires soldered to the terminals, see Figure 6.

Crack gauges were not used for the 'wet' fatigue testing as they require a coating of polyurethane varnish to prevent short circuiting by the water. This prevents water gaining access to one side of the bondline, and reduces the rate of water uptake compared with a non-gauged specimen[14].

5.4.3 Experimental Procedure

The gauge was connected to the 'Fractomat', see Figure 7. This provides the constant current supply to the gauge and displays the distance that the crack has propagated into the gauge. The constant current supply was adjusted using the potentiometer on the front panel until the crack length display read zero. The distance from the loading point to the active part of the gauge was measured with a vernier calliper. Though the 'Fractomat' displays the crack length in millimetres, the output to the 'MacLab' is in volts, and so a conversion must be set on the computer so that the software gives a reading in millimetres. The signal from the 'Fractomat' was sampled from the computer software, and set to the measured crack length. Two values are required to convert from voltage to crack length, so the potentiometer was adjusted to read 90 mm, and sampled again. This sets the conversion from voltage to crack length, and the 'Fractomat' was zeroed again.

The load values must be converted in a similar manner. The specimen was placed in the testing machine and the slack in the pins taken up. The output voltage from the load cell was sampled from the computer software, providing one conversion value. The mean displacement was applied to the specimen, and the cyclic loading superimposed. The load was sampled again, and the maximum value used as the second conversion value. Thus the computer gives the load in Newtons and crack length in millimetres as a function of the number of cycles. One second samples were taken at intervals of between 1 minute and 2 hours. Samples were taken more frequently at the beginning of the test when the crack growth rate was higher. The data were analysed to give the maximum load and crack length in each data sample. Values of G_{max} and da/dN were calculated using the equations in section 5.2

5.4.4 Gauge Results

The crack lengths measured via the optical and potential drop methods agreed well, as shown in Figure 8. However problems were encountered at longer crack lengths on some of the 'AV119'/steel specimens. Figure 9 shows a plot of compliance (δ_{max}/P_{max}) versus crack length for one of these specimens. The TDCB specimen is designed such that this relationship is linear, but the increase in crack length indicated by the increase in compliance, and seen optically, is not recorded accurately by the potential drop method. This problem was only encountered on the 'AV119'/steel specimens, the stiffest specimens used, at small maximum displacement values. Thus it is suggested that the problems may be due to the gauge not breaking, or the broken halves of the gauge staying in contact, due to the small displacement. However, in most cases no problems were observed with the crack gauges. Problems with the gauges can be identified by the deviation from the linear response, as shown in Figure 9, or from comparisons with the optical measurements of the crack length taken with a travelling microscope.

5.5 RESULTS

5.5.1 Introduction

The results from the fatigue TDCB tests were plotted as graphs of the rate of crack growth, da/dN, against maximum fracture energy, G_{max}, using log-log axes. All the tests showed evidence of a threshold fracture energy, G_{th}, below which crack growth does not occur. These values, and the apparent loci of joint failure obtained from examination by optical microscopy, are given in Tables 3a & 3b for the 'AV119' and 'F241' adhesives respectively.

The fracture surfaces were analysed using Auger Electron Spectroscopy (AES) and X-ray Photoelectron Spectroscopy (XPS)[15], to identify their elemental composition. The first technique is more suited to aluminium specimens, and provides good spatial resolution as the analysis area is 100 μm in diameter. The XPS data is taken over an area which is 5 mm in diameter, but this technique is more suitable for the analysis of the steel specimens than the AES.

Depth profiling was also used with the above techniques. The surface is eroded to a known depth by ion bombardment, and then analysed. Thus any changes in the composition with depth can be identified. The depth profile of the AES could be calibrated, and so the depth at which analyses were carried out is known. However the XPS data could not be calibrated and so only an etch time is quoted.

Contamination of the fracture surfaces by silicon was observed by both AES and XPS with some specimens. This is probably due to decomposition of the silicone sealant used to seal the joints in the water tanks.

5.5.2 Diffusion of Water into Adhesive Joints

Before the durability results are discussed it is useful to consider how much water will have diffused into the joints during the 'wet' tests. As described in section 2.3 above, water can enter a joint by diffusion through the adhesive or by permeating along the interface. The first of these processes can be modelled using Fick's second law of diffusion[3]. This allows the concentration of water at any point in a joint to be found after a time 't'. Data was obtained for the 'AV119' adhesive samples under task 5 of project 3 of the MTS Programme[3]. Samples of bulk adhesive were immersed in water, held at a constant 60°C. They were removed at intervals and weighed.

This enabled the diffusion coefficient of the adhesive to be calculated. Hence, the concentration of water at a given point in any joint can be found[2].

A typical 'wet' test lasted for about 6 x 10^6 cycles, equivalent to 14 days of water immersion. Using the data above, it is possible to calculate the water concentration profile within the joint after this time, see Figure 10. The concentration of water at the edge of the joint will be 100 %. After 6 x 10^6 cycles, points at a distance of less than 1 mm in from the edge of the joint would have a water concentration of more than 50 % of saturation. After 16 x 10^6 cycles, the longest test time used, water would have reached the centreline of the joint, about 2 % being present there.

A value for the diffusion coefficient is only available for the 'AV119' adhesive, and at 60°C. At this temperature diffusion would be expected to be more rapid than at the 28°C used in the durability tests. However interfacial diffusion tests showed an increased diffusion rate compared to bulk samples[4].

5.5.3 'AV119'

5.5.3.1 Chromic-Acid Etched Aluminium

The aluminium alloy specimens with the CAE surface treatment failed in a cohesive-in-adhesive manner in 'dry' fatigue, with a threshold value, G_{th}, at 160 J/m^2, Figure 11. This compares with a G_C value of 700 J/m^2 from the static tests. Thus the cyclic loading has reduced the fracture energy by a factor of 4.

For the 'wet' tests apparently interfacial failure was observed, see Figure 12, and a threshold value of 175 J/m^2 was recorded. The surface analyses performed by AES have shown aluminium oxide on both surfaces, see Table 4. This indicates that failure was through the oxide, but with residual adhesive also present. Table 4 also shows that there is a thick layer of aluminium oxide present after the CAE treatment. At a depth of 40 nm on the metal side no elemental aluminium is detected.

5.5.3.2 Gritblast/Degreased Aluminium

Specimens using the GB/DG treated aluminium substrates failed apparently interfacially when tested 'dry' or 'wet', as shown in Figure 13. The threshold fracture energies obtained were 85 and 25 J/m^2 respectively, see Figure 14.

The surface analyses performed on one of the specimens after 'dry' testing indicated that failure occurred within the aluminium oxide, Table 5. The results at zero depth on the adhesive side are likely to be from surface contamination, as 100 % carbon was detected. Elemental aluminium is detected at a depth of 16 nm on the metal side (area A). This shows that the oxide layer is much thinner than with the CAE treatment above, where no elemental aluminium was detected at 40 nm depth.

The AES results, shown in Table 6, for the 'wet' specimen indicate that failure occurs through the aluminium oxide, with some residual adhesive.

5.5.3.3 Steel

'Dry' fatigue of the 'AV119'/steel specimens gave an apparently interfacial failure locus, as shown in Figure 15. A threshold value, G_{th}, of 50 J/m^2 was measured, see Figure 16. Surface

analysis was performed on a 'dry' specimen using XPS, and the results are shown in Table 7. These indicate that failure is cohesive-in-adhesive, but close to the interface.

The 'wet' fatigue tests gave a value of 35 J/m^2, when failure was apparently interfacial, see Figure 16b. The 'wet' specimens exhibited a considerable amount of corrosion on both of the fracture surfaces. This would seem to indicate that here the failure was within the oxide layer on the surface of the steel, see Figure 17. However some specimens did not show uniform corrosion, as shown in Figure 18. The cream areas amongst the brown/black corrosion would seem to be residual adhesive. Hence these specimens have failed partly cohesively, and gave a threshold value of 20 J/m^2. The gross corrosion seemed to be a post-failure effect, as areas well ahead of the crack tip showed no discoloration. However, some discoloration was observed in the area directly in front of the crack tip, see Figure 18. This would indicate that water is permeating along the interface faster than through the bulk adhesive.

5.5.3.4 Summary

All the 'AV119' data obtained is collected together in Figure 19, and Table 3a. These show that the fatigue performance of the CAE treated aluminium alloy specimens is relatively unaffected by the water immersion, compared with the GB/DG treatment. The 'dry' threshold for the GB/DG treatment is half that for the CAE, the values being 85 and 160 J/m^2 respectively The water immersion reduces the threshold value for the GB/DG treatment, from 85 to 25 J/m^2. The steel specimens gave a G_{th} value of 55 J/m^2 when tested 'dry', and 20 J/m^2 in the 'wet' environment.

5.5.4 'F241'

5.5.4.1 Chromic-Acid Etched Aluminium

The TDCB tests with chromic-acid etched substrates gave a threshold of 140 J/m^2 for the 'dry' tests, see Figure 20. All failures were cohesive-in-adhesive, as shown in Figure 21. However there is more scatter in the measured values than was observed in the 'AV119' tests, see Table 3.

The 'wet' specimens exhibited mixed failure types, see Table 3b. Cohesive-in-adhesive failure, see Figure 22, gave a threshold value of 140 J/m^2. Where apparent interfacial failure occurred it was along the edge of the specimen, see Figure 23, and a higher value of G_{th} was measured. A value of 270 J/m^2 was obtained for 10 % apparently interfacial failure. Table 8 shows the AES results from this area of apparently interfacial failure. These show that failure is through the aluminium oxide, with some residual adhesive on the fracture surfaces. Significant discoloration of the exposed fracture surfaces was noted on this specimen, as shown in Figure 23, when broken open after 16 x 10^6 cycles. The failure was mostly cohesive-in-adhesive, with some failure in the oxide at the edges. The unfractured part of this joint did not show any discoloration, as did other specimens immersed for up to 6 x 10^6 cycles.

5.5.4.2 Gritblast/Degreased Aluminium

The specimens tested 'dry' failed cohesively in the adhesive and gave a threshold value of 200 J/m^2, see Figure 24. One specimen was allowed to fatigue for 12 x 10^6 cycles to investigate whether the threshold value would fall any further. A decrease of about 10 J/m^2 was observed, but this still lies within the experimental scatter.

The 'wet' testing produced either apparently interfacial or partially cohesive failure. Where failure was apparently interfacial, see Figure 25, the threshold was 25 J/m^2, but was 60 J/m^2 where areas of cohesive failure could be seen by optical microscopy, as shown in Figure 26.

Analysis of the apparently interfacial areas of the fracture surfaces by AES, see Table 9, showed that there was failure through the aluminium oxide, but with residual adhesive on the surfaces.

5.5.4.3 Steel

The steel specimens bonded with 'F241' failed in a cohesive-in-adhesive manner when tested 'dry', and gave a threshold at 95 J/m^2, see Figure 27. Areas of apparent interfacial failure were identified by optical microscopy, similar to those seen with the CAE aluminium alloy specimens above, as shown in Figure 22b. However analysis by AES and XPS, see Table 10, showed that the failure was cohesive-in-adhesive. Thus all the 'dry' tests exhibited cohesive-in-adhesive failure.

A similar apparent interfacial failure was observed on the fracture surfaces of the specimens that were tested in the 'wet' environment. Here the failure at the edges was within the oxide, as indicated by the presence of corrosion on both surfaces, see Figure 28. This is confirmed by the XPS analysis, Table 11. Note that the XPS analysis covers areas of cohesive-in-adhesive and apparently interfacial failure, see Figure 29. The failure was cohesive in the adhesive across most of the width of the specimen. The threshold value of fracture energy was found to be 50 J/m^2.

5.5.4.4 Summary

The 'F241' specimens exhibited mostly cohesive-in-adhesive failure, with some apparently interfacial failure at the edges of the specimens. This could have a significant effect on the measured threshold, as shown in Table 3b. The CAE specimens showed cohesive-in-adhesive failure with a G_{th} value of approximately 140 J/m^2, both 'dry' and 'wet'. The data from the aluminium tests are shown in Figure 30. The GB/DG treatment shows a significant decrease in fracture energy upon water immersion, from 200 J/m^2 when 'dry' to a 'wet' value of 25 J/m^2. Water immersion also reduced the threshold value for the steel specimens from 95 J/m^2 for the 'dry' tests to a 'wet' value of 50 J/m^2, see Figure 27. The G_{th} value for the steel specimens is lower than that for the aluminium specimens because failure occurs very close to the substrates. The difference between the G_{th} values for the CAE and GB/DG aluminium specimens could be accounted for by scatter in the data. However, more G_{th} values are required than could be generated in the time available.

5.5.5 Discussion

Water has been shown to reduce the fatigue resistance of both adhesives when used on steel substrates. The cohesive-in-adhesive threshold values obtained from the CAE aluminium alloy specimens have been largely unaffected by the presence of water, probably because this treatment produces a chemically stable oxide layer. By contrast the oxide layer after GB/DG treatment is thinner and less stable, thus failure can occur more easily through the oxide and results in a reduction in the measured value of G_{th}.

Previous work on bonded aluminium TDCB specimens[14] has used transmission electron microscopy (TEM) to investigate the thickness of the oxide layer at and just ahead of the crack tip. This concluded that a subtle process of hydration/corrosion was occurring, which was sufficient to weaken the oxide, but not to show up as gross hydration, and hence thickening of the layer.

The steel specimens do not exhibit corrosion in areas well ahead of the crack tip, thus indicating that water entering from the edge of the joint is not the governing factor. The action of

opening and closing the joint will pump water into the crack tip. Once water has access to the interface here it can permeate along the interface, and weaken this region.

More scatter was observed in the 'F241' data than those from the 'AV119'. This may be due to variable proportions of hardener and resin being present in the acrylic adhesive.

The gaps in the data between the highest value of G_{max} from the fatigue tests is due to a single crack propagation and arrest from the starter foil at the beginning of the test. Thus the fatigue data starts from a lower value of G_{max} and leaves an interval over which data cannot be obtained.

5.6 CONCLUSIONS

The results are summarised in Table 12. The fatigue tests of the TDCB specimens has shown that for both adhesives, and all the surface treatments, there is a threshold value of the fracture energy, G_{th}. This is where the crack growth rate becomes vanishingly small, of the order of 0.01 mm in a million cycles. The value of this threshold depends on both the adhesive and the substrate/surface treatment combination used, as apparently interfacial failure can occur. Water immersion reduces the threshold value for the GB/DG surface treatment on both the aluminium alloy and steel substrates. However, for the CAE treated aluminium-alloy the value of G_{th} is largely unaffected.

Substrate & Surface Treatment	'Dry'			'Wet'		
	Failure Locus	G_{th}, J/m^2	Range, J/m^2	Failure Locus	G_{th}, J/m^2	Range, J/m^2
CAE Aluminium	C	**160**	±10	I	**175**	±20
GB/DG Aluminium	I	**85**	±3	I	**25**	±2
GB/DG Steel	I	**55**	±10	O	**35**	-
				O+C	**20**	±2

3(a) 'AV119' adhesive.

Substrate & Surface Treatment	'Dry'			'Wet'		
	Failure Locus	G_{th}, J/m^2	Range, J/m^2	Failure Locus	G_{th}, J/m^2	Range, J/m^2
CAE Aluminium	C	**130**	±30	C	**140**	-
				C+I	**270**	±30
GB/DG Aluminium	C	**200**	±15	I	**25**	±3
				C+I	**60**	±1
GB/DG Steel	C	**95**	±15	C+O	**50**	±2

3(b) 'F241' adhesive

Note Failure loci;

C: Cohesive in the adhesive.
I: Apparently interfacial.
O: Oxide.
C+I ⎫ Mixed failure, first term predominates.
O+C ⎭

Table 3. *Apparent locus of failure (optical) and threshold fracture energy, G_{th}, values from TDCB cyclic fatigue tests, (a) 'AV119' adhesive, (b) 'F241' adhesive. Where several specimens failed with the same failure locus the range of threshold values is given.*

	Area	Depth, nm	Al(o)	Al(e)	C	N	O
'Metal' Side	A	0	16.5	0	25.0	0	57.4
	A	14	23.9	0	31.8	0	44.3
	A	43	23.5	0	36.2	0	40.2
	B	0	2.9	0	58.3	2.7	35.5
	B	13	23.2	0	31.8	0	44.0
	B	42	25.2	0	30.0	0	44.9
'Adhesive' Side	A	0	4.1	0	63.8	0	30.5
	A	14	21.5	0	38.1	0	40.0
	A	41	8.4	0	60.6	0	31.1
	A	75	4.4	0	77.3	0	18.3
	B1	0	3.9	0	56.0	2.0	36.2
	B2	0	31.5	0	13.7	0	53.5

Note
1. Al(o) is the percentage of aluminium in the form of oxide, Al(e) is the percentage of aluminium in the elemental form.
2. The area 'A' on one fracture surface is approximately opposite 'A' on the other.
3. Si, S < 1.0 %, Cl <2.0 %.

Table 4. *AES results for 'wet' 'AV119'/CAE aluminium fatigue specimens, showing elemental composition by atomic percentage.*

	Area	Depth, nm	Al(o)	Al(e)	Mg	C	N	O
'Metal' Side	A	0	7.2	0	21.4	30.0	1.2	38.4
	A	16	7.5	64.4	6.9	6.9	0	14.3
	A	48	3.4	82.1	0	6.1	0	8.4
	B	0	12.5	0	20.6	19.9	0	45.1
'Adhesive' Side	A	0	0	0	0	100	0	0
	C	0	0	0	0	100	0	0

Note
1. Al(o) and Al(e) are the percentages of aluminium in the oxide and elemental forms respectively.
2. Si & S < 1.1 %.

Table 5. *AES results for 'dry' GB/DG aluminium specimens bonded with 'AV119'.*

	Area	Depth, nm	Al(o)	Al(e)	Si	C	O
'Metal' Side	A	0	29.3	0	0	10.1	59.0
	B	0	31.7	0	1.1	9.5	57.1
	C	0	34.5	0	0.6	7.2	56.9
	C	8	38.0	0	1.0	3.1	57.2
	C	32	29.9	15.7	0.5	3.7	49.2
	C	64	21.0	44.1	0	2.9	32.1
	C	96	16.2	56.8	0	3.3	23.7
	C	160	12.0	67.9	0	2.7	17.4
'Adhesive' Side	A	0	31.4	0	0	9.8	58.4
	B	0	25.9	0	1.1	17.2	55.3
	B	16	31.7	0	0	9.5	58.8
	B	48	31.9	0	0	9.0	59.2
	B	112	30.5	0	0	10.5	59.0

Note
1. Al(o) and Al(e) are the percentages of aluminium in the oxide and elemental forms respectively.
2. S < 1 %, Cl < 0.7 %.

Table 6. *Surface analysis results from AES of GB/DG aluminium specimens bonded with 'AV119', fatigue tested in 'wet' environment.*

	Etch Time	Fe	Si	C	N	O
'Adhesive' Side	0	0	3.7	73.7	2.8	19.3
	60	0	2.6	82.7	2.9	10.2
	130	0	2.0	75.0	2.8	8.8
	300	0	2.3	87.6	2.3	6.8
	1500	0	1.9	87.7	3.1	6.2
'Metal' Side	0	0	4.5	65.5	2.0	28.0
	1500	19.7	0	58.7	5.0	16.6

Note
The etch times could not be calibrated, and so the depth at which the analyses were conducted cannot be quoted, however a rough estimate of the etch rate would be 1 nm/min. At this rate an etch time of 1500 s would give a depth of 25 nm.

Table 7. *XPS results for 'dry' steel specimens bonded with 'AV119', showing elemental composition by atomic percentage.*

	Area	Depth, nm	Al(o)	Cl	C	O
'Metal' Side	A	0	23.3	8.2	20.3	48.0
	B	0	42.9	0.0	0.0	57.1
	C	0	26.1	7.6	17.0	48.4
	C	16	27.7	3.3	34.8	34.3
	C	48	10.4	4.3	58.9	26.4
'Adhesive' Side	A	0	39.3	0.0	4.0	56.7
	A	16	33.8	0.0	2.8	63.4
	A	48	38.6	0.0	2.2	59.2
	B	0	22.2	8.0	18.6	51.2
	C	0	40.2	0.0	3.8	56.0

Note
S < 0.3 %.

Table 8. *AES results for 'wet' 'F241'/CAE aluminium specimens for area of apparent interfacial failure. Elemental composition by atomic percentage.*

	Area	Depth, nm	Al(o)	Al(e)	Mg	Si	Cl	C	O
'Metal' Side	A	0	20.8	0	10.0	4.0	0.6	7.5	56.8
	B	0	15.0	0	15.7	2.4	1.0	12.5	52.7
	B	8	28.8	0	14.8	1.2	0	3.7	51.5
	B	16	36.0	0	10.8	0	0	3.7	49.5
	B	32	22.4	27.1	10.1	0	0	4.0	36.3
	B	48	19.5	25.4	6.5	0	0	9.7	38.9
	B	80	15.9	50.0	0	0	0	7.9	26.3
	C	0	18.3	0	0	0	1.2	18.4	61.4
	C	80	36.7	1.3	0	0	0	2.8	59.2
	C	160	31.9	10.9	0	0	0	2.7	54.5
'Adhesive' Side	A	0	0	0	0	0	5.8	76.1	18.1
	D	0	22.2	0	0	0	4.6	21.4	51.7
	E	0	20.7	0	0	0	3.5	22.4	53.5

Note
Al(o) and Al(e) are the percentages of aluminium in the oxide and elemental forms respectively.

Table 9. *AES results for 'wet' GB/DG aluminium specimens bonded with 'F241', for area of apparent interfacial failure. Elemental composition by atomic percentage.*

	Depth, nm	Fe	Si	Cl	S	C	N	O
'Metal'	0	0	19.2	1.7	1.9	32.2	2.3	42.8
Side	1.6	0	2.3	1.4	1.0	56.2	0	36.9
	5	0	2.0	1.8	1.3	74.0	0	19.2
	20	0	0	2.0	0.9	76.7	0	17.8
	50	0	0	4.5	0	80.9	0	12.3
'Adhesive'	0	0	8.7	4.5	0.6	53.0	4.0	29.1
Side	5	0	0	2.8	1.1	88.7	0	7.4

a) AES analysis.

	Etch Time, s	Fe	Si	Cl	C	N	O
'Metal'	0	0	8.7	4.9	66.4	1.7	18.3
'Adhesive'	0	0	8.1	6.2	66.8	1.1	17.9

b) XPS analysis.

Note
Analysis area is apparently interfacial optically. However the surface analysis results show that failure is cohesive-in-adhesive.

Table 10. *Surface analysis results for steel specimens bonded with 'F241', tested in the 'dry' environment, for area of apparent interfacial failure, (a) AES analysis, (b) XPS analysis.*

	Depth, nm	Fe	Cl	C	O
'Metal'	0	1.6	1.8	86.4	10.1
'Adhesive'	0	3.1	3.2	74.2	18.3

Note
See Figures 28 & 29 for identification of analysis area.

Table 11. *XPS results for 'wet' 'F241'/steel specimens, showing elemental composition by atomic percentage.*

Substrate & Treatment & Treatment	Static Fracture Energy, G_C, J/m^2	Threshold Fracture Energy, G_{th}, J/m^2	
		'Dry'	'Wet'
CAE Aluminium	700 C	160 C	175 O+C
GB/DG Aluminium	520 C	85 I+O	25 O
GB/DG Steel	450 C+I	55 C	20 O+C

a) 'AV119' adhesive.

Substrate & Treatment	Static Fracture Energy, G_C, J/m^2	Threshold Fracture Energy, G_{th}, J/m^2	
		'Dry'	'Wet'
CAE Aluminium	820 C	130 C	140 C+O
GB/DG Aluminium	820 C	200 C	25 C+O
GB/DG Steel	840 C	95 C	50 C+O

b) 'F241' adhesive.

Note

1. Where two threshold fracture energies were found, for different apparent failure loci, the lower value is quoted.

2. Failure loci:

C: Cohesive in the adhesive.
I: Interfacial.
O: Oxide.
C+O Mixed failure, first term predominates.
I+O Mixed failure, first term predominates.

Table 12. Summary of fatigue test data from TDCB tests, with locus of failure from optical and surface chemical analysis.

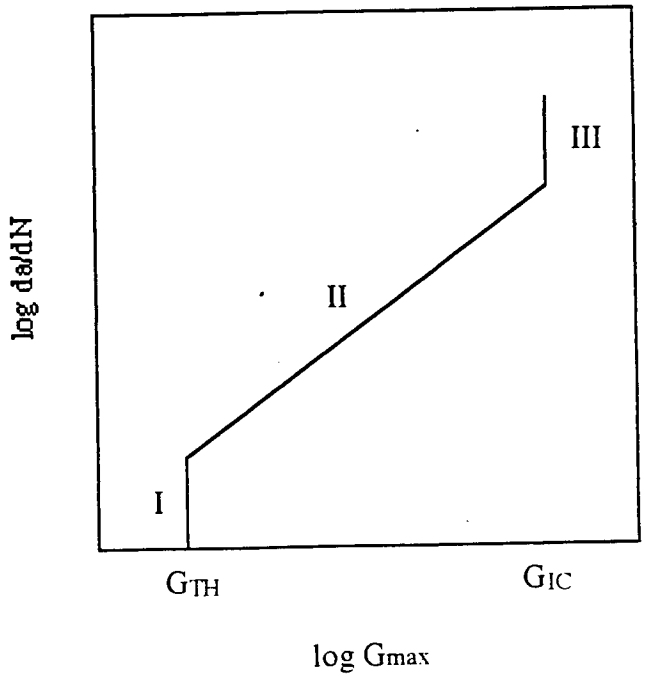

Figure 5. **Typical plot of logarithmic crack growth rate per cycle, da/dN, versus logarithmic maximum applied fracture energy, G_{max}.**

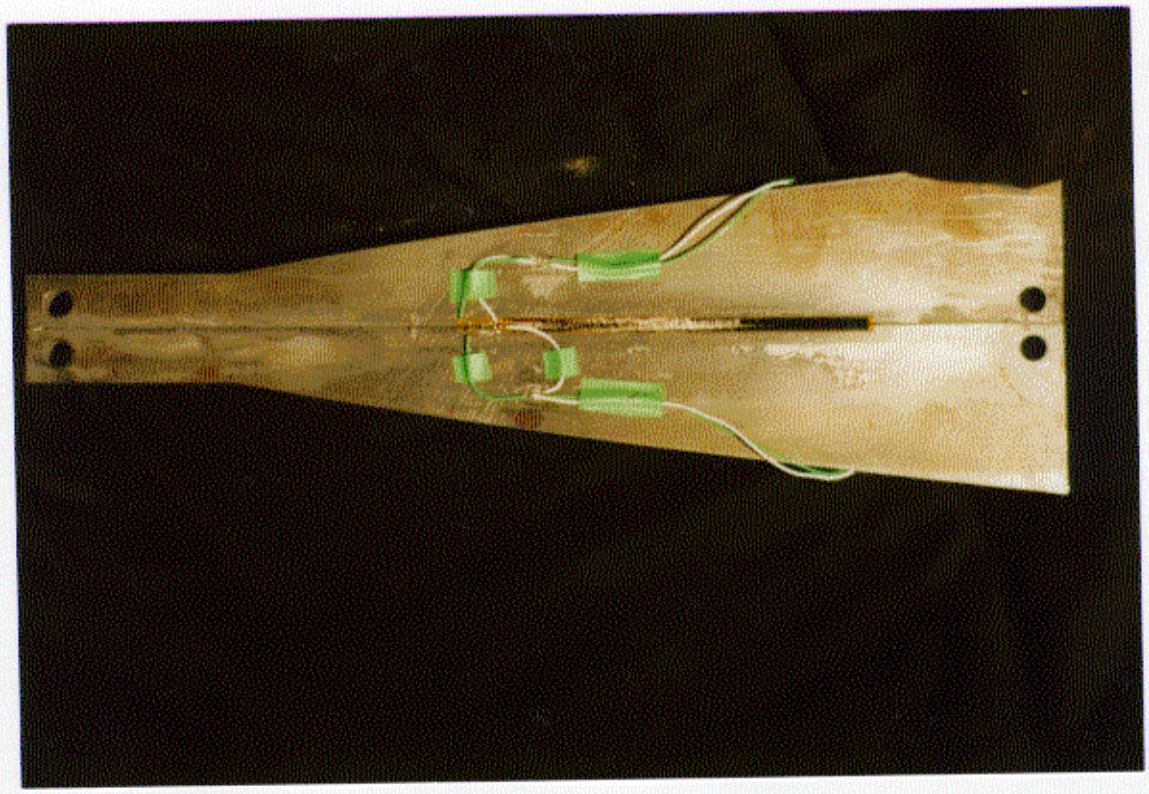

Figure 6. **The Rumul S100 crack gauge.**

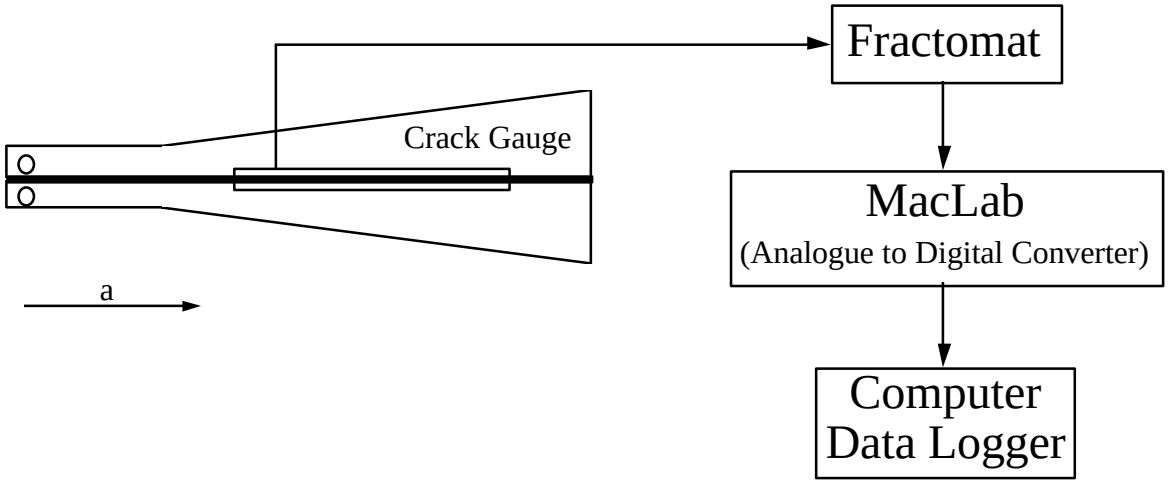

Figure 7. Crack gauge system schematic.

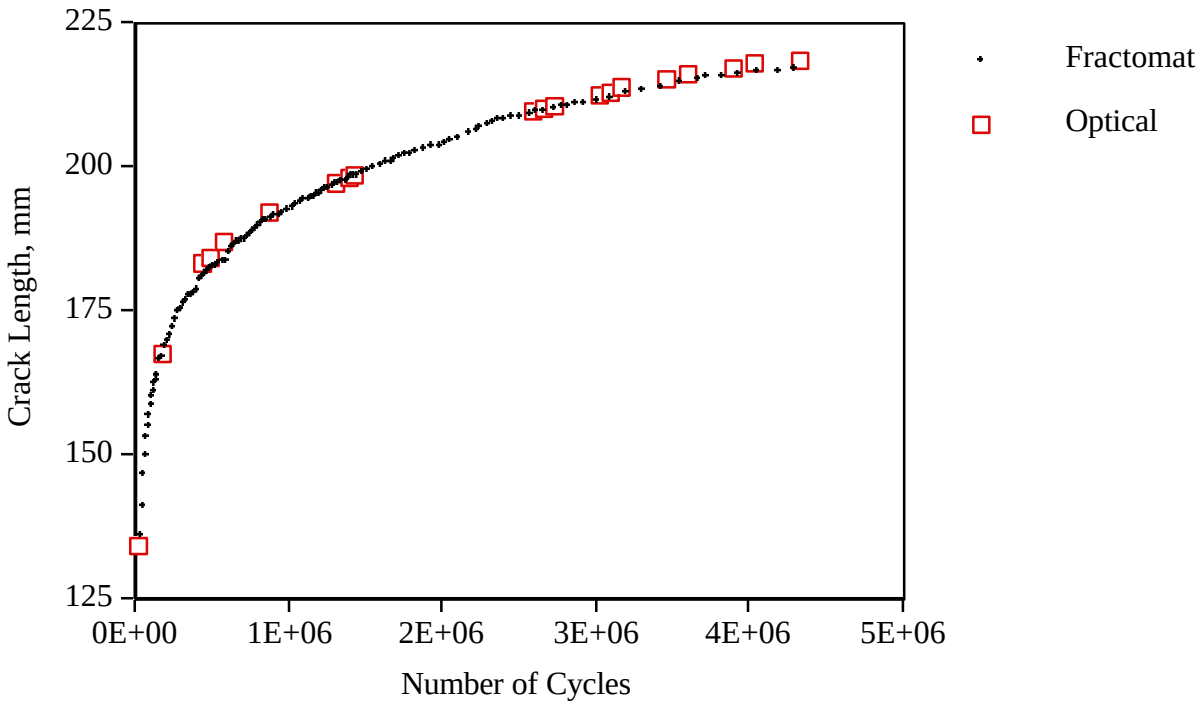

Figure 8. **Comparison of crack length measurements by optical and potential drop methods. Note excellent agreement between the two methods.**

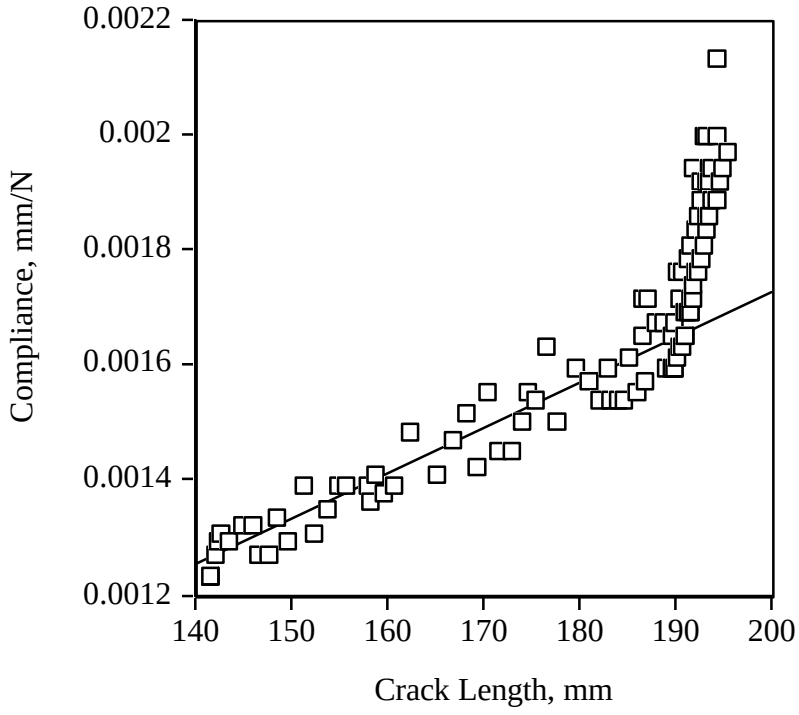

Figure 9. **Compliance versus crack length from crack gauge showing deviation from linear response caused by gauge failing to register increase in specimen crack length.**

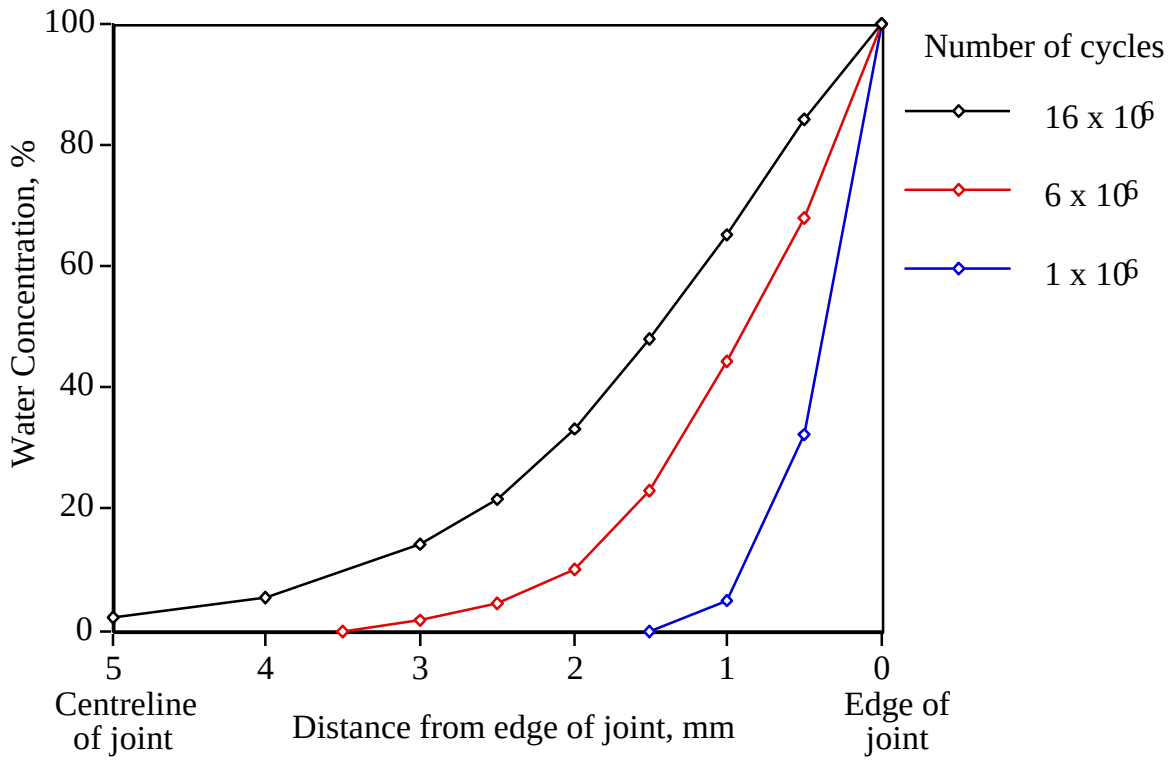

Figure 10. Water concentration distributions for 'AV119' adhesive at various water immersion times, calculated from 60°C diffusion data[3], after[2].

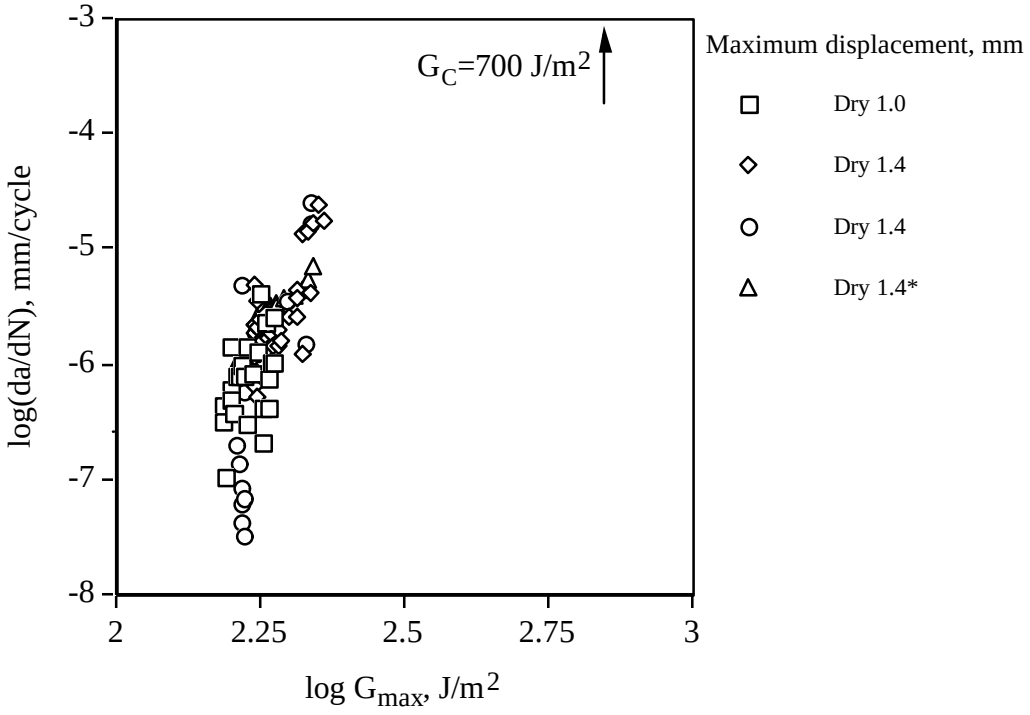

(a) 'Dry', (* denotes crack gauge data, otherwise from travelling microscope measurements).

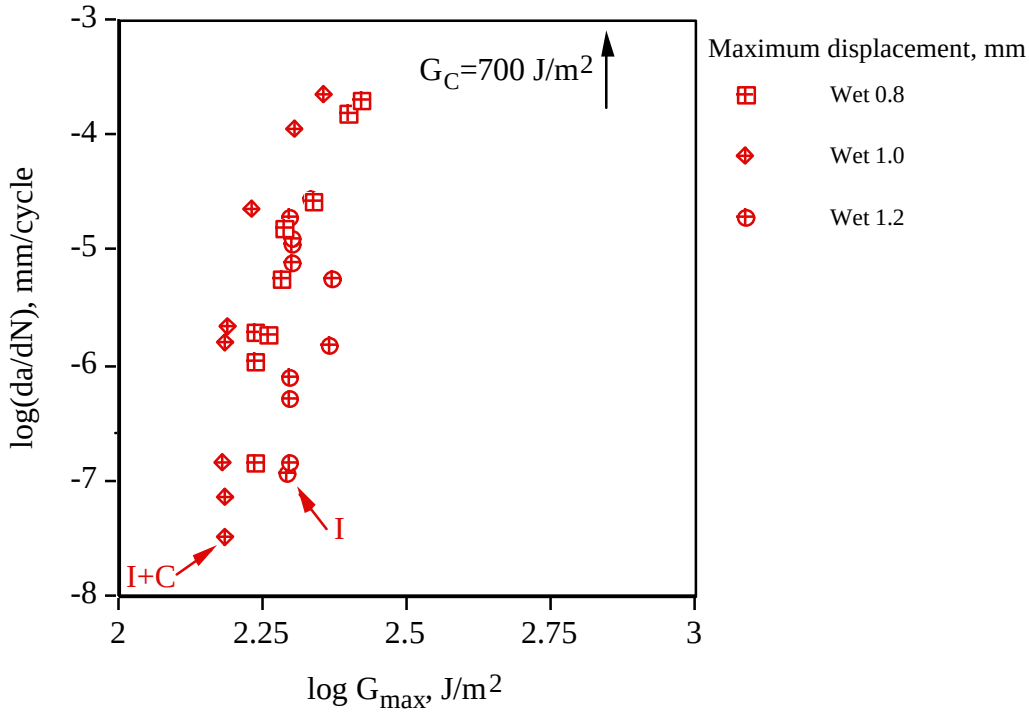

(b) 'Wet'

Figure 11. Rate of crack growth versus applied maximum fracture energy for 'AV119' adhesive with chromic-acid etched aluminium substrates, (a) 'Dry', (b) 'Wet'.

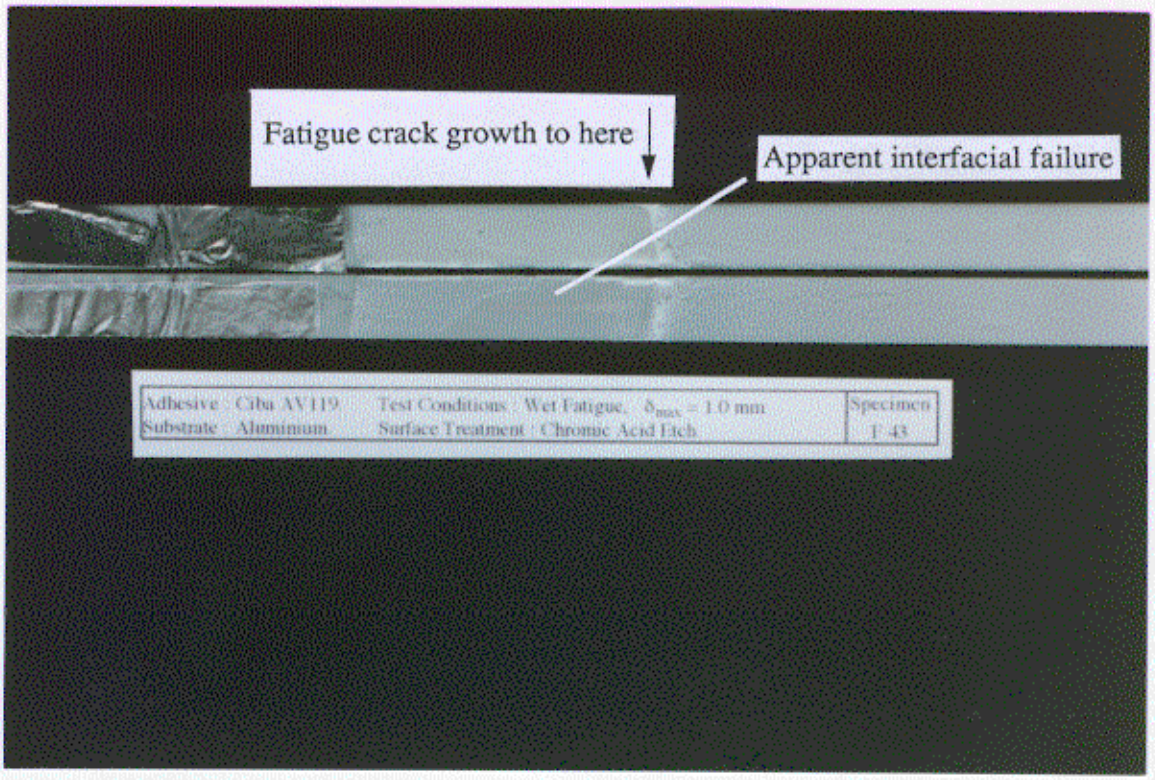

Figure 12. **Fracture surface of CAE aluminium specimen bonded with 'AV119', tested 'wet', showing apparent interfacial failure.**

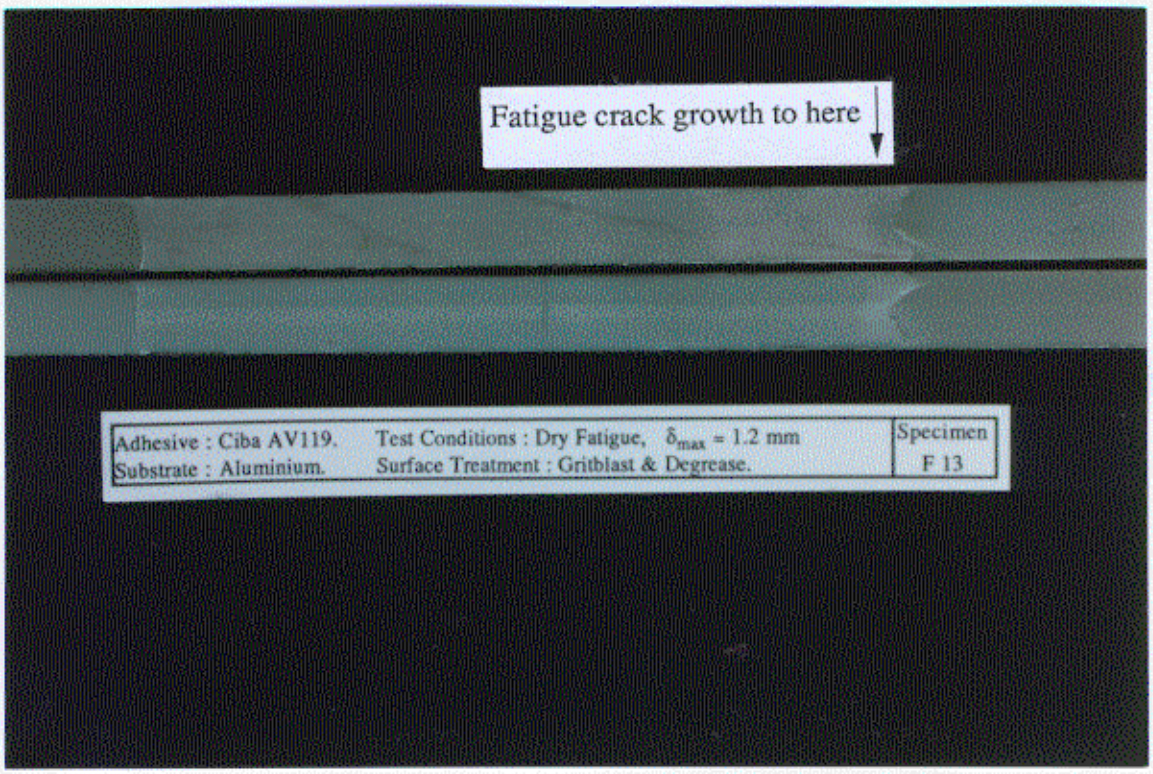

Figure 13. **Fracture surface of aluminium alloy specimen bonded with 'AV119', gritblast & degrease surface treatment, tested 'dry', showing apparently interfacial failure.**

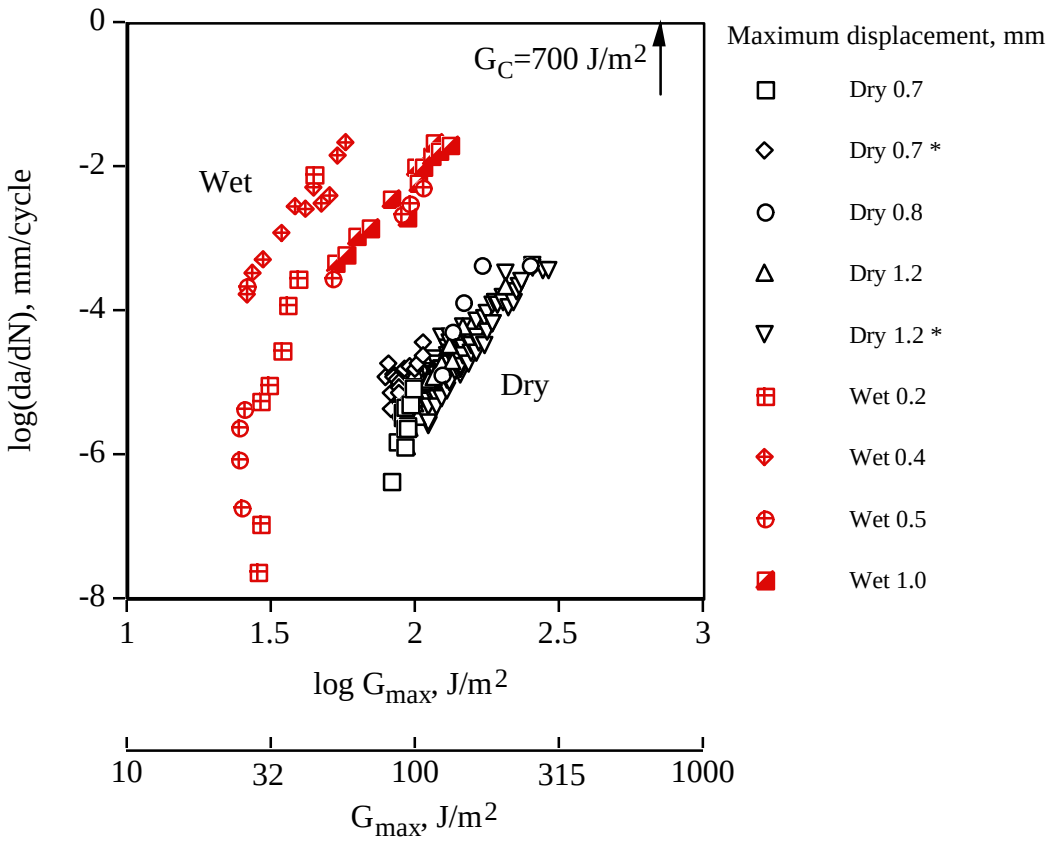

Figure 14. Rate of crack growth versus applied maximum fracture energy for 'AV119' adhesive with gritblast/degrease aluminium substrates, (* denotes crack gauge data).

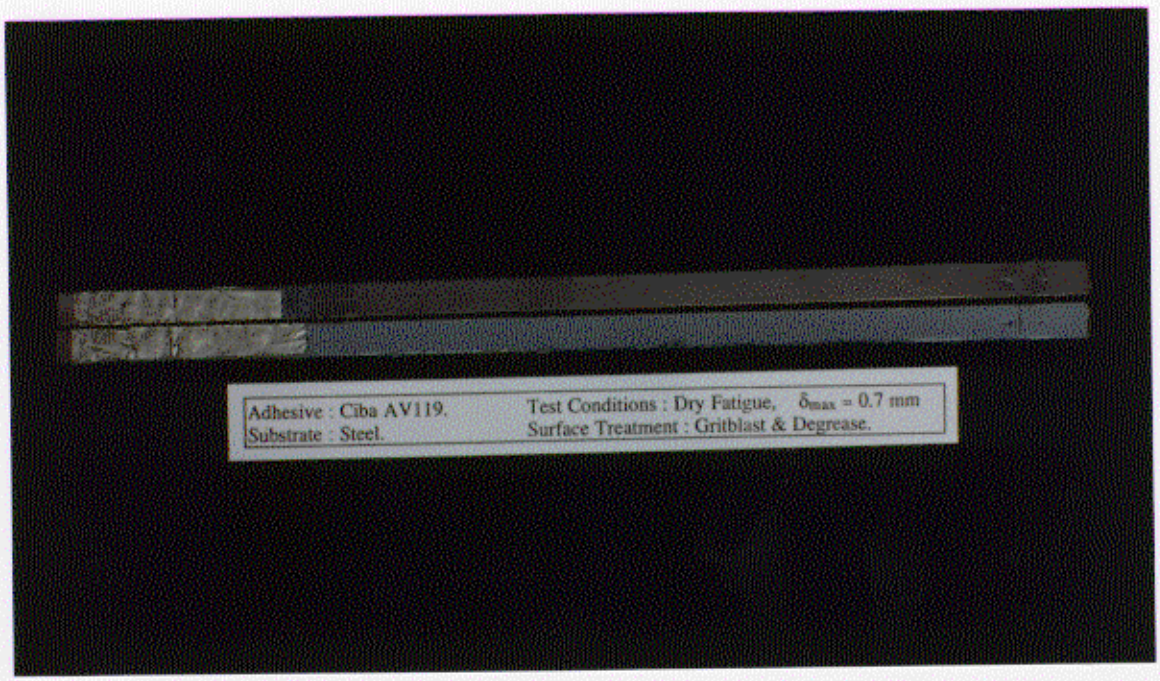

Figure 15. Fracture surface of 'dry' steel specimen bonded with 'AV119' showing apparently interfacial failure.

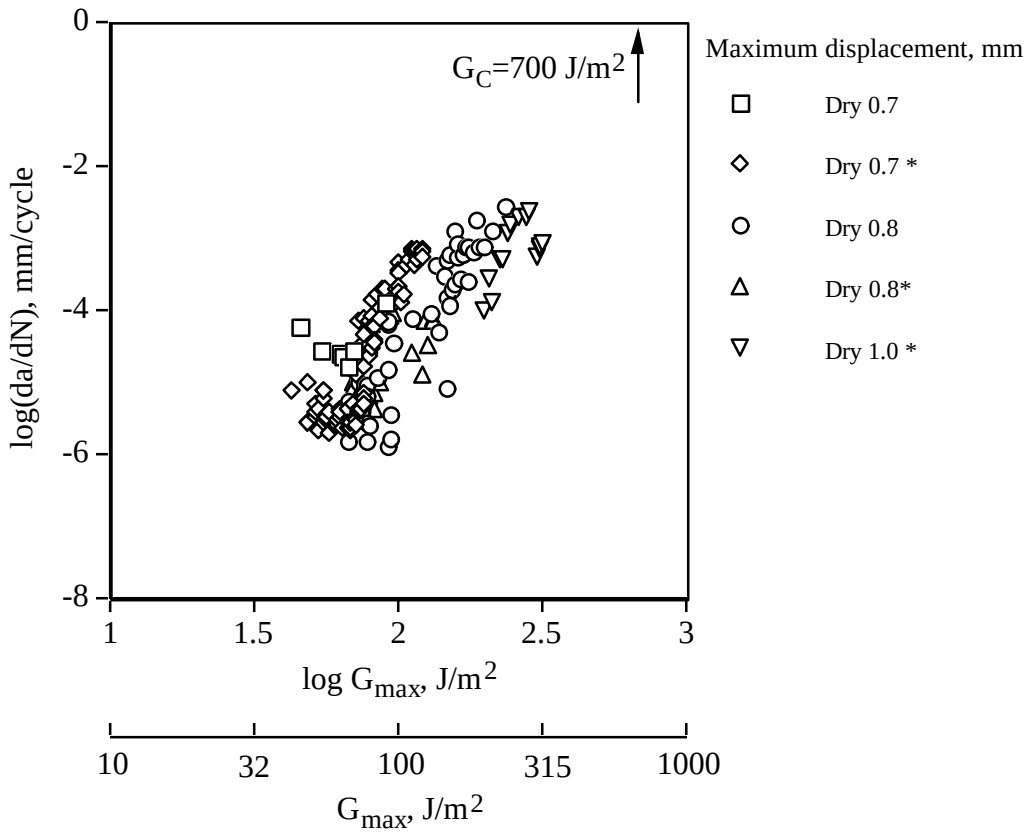

(a) 'Dry', (* denotes crack gauge data, otherwise from travelling microscope).

Figure 16. Rate of crack growth versus applied maximum fracture energy for steel substrates bonded with 'AV119' adhesive, (a) 'Dry', (b) 'Wet'.

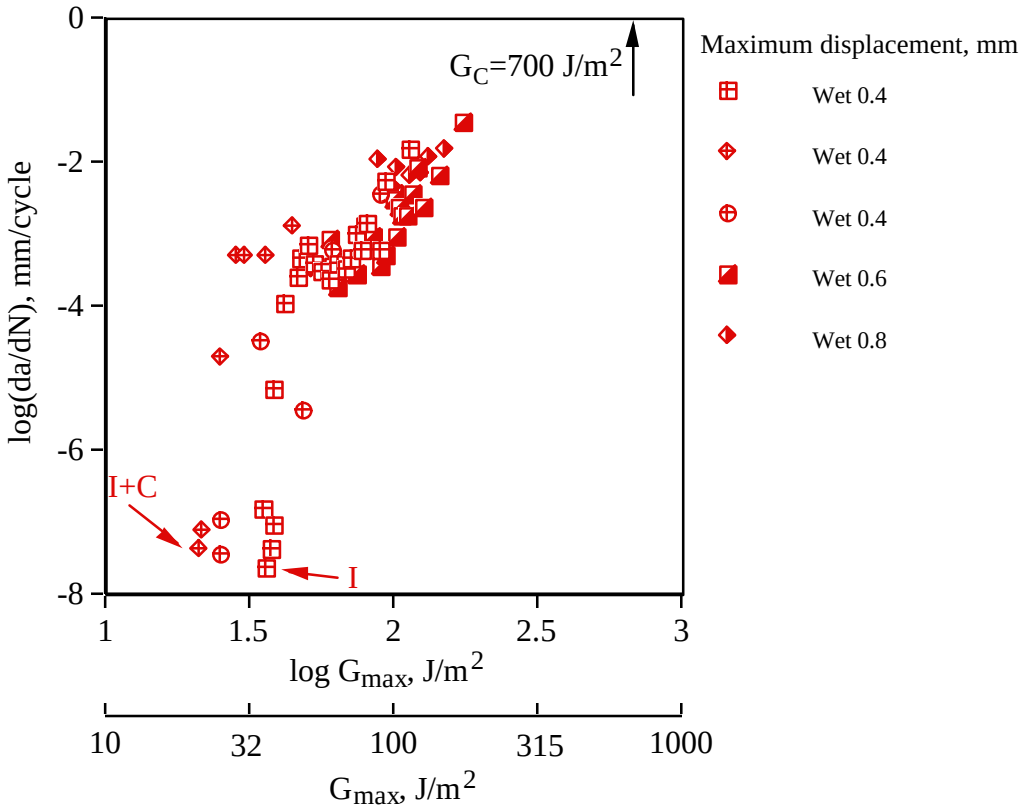

(b) 'Wet'.

Figure 16. Rate of crack growth versus applied maximum fracture energy for steel substrates bonded with 'AV119' adhesive, (a) 'Dry', (b) 'Wet'.

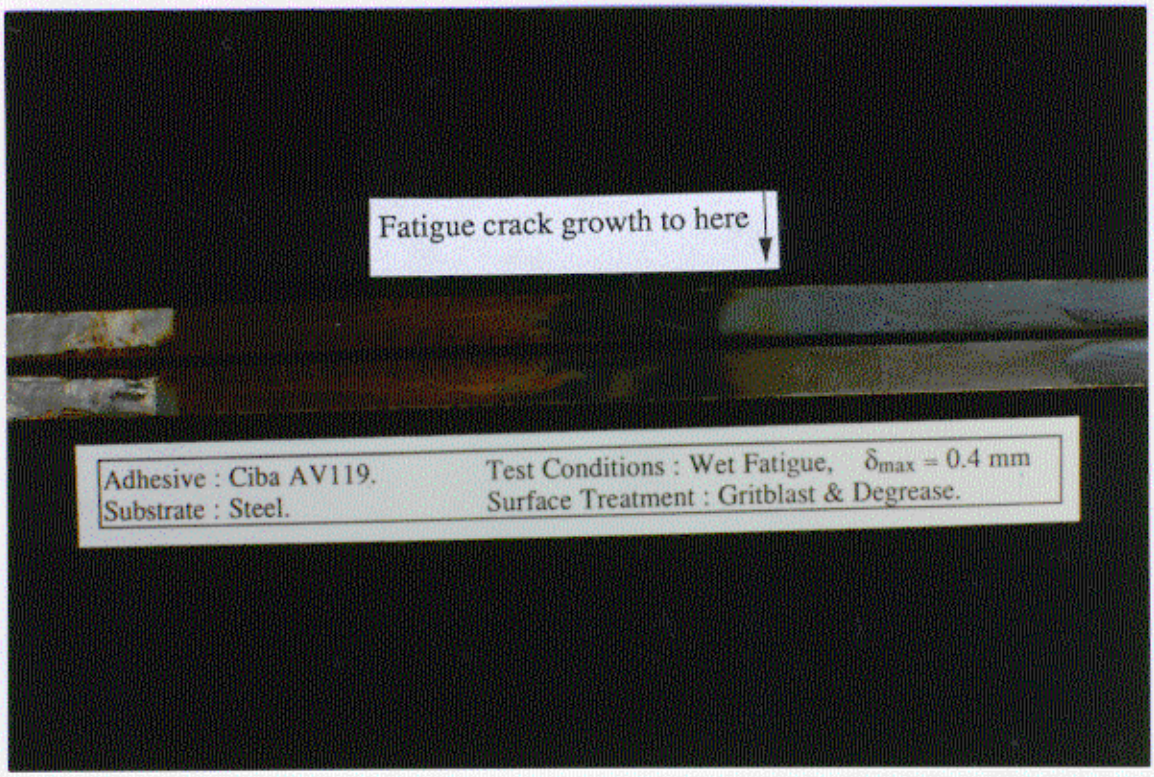

Figure 17. **Fracture surface of 'wet' steel specimen bonded with 'AV119' showing apparently interfacial failure and corrosion of exposed oxide on both fracture surfaces.**

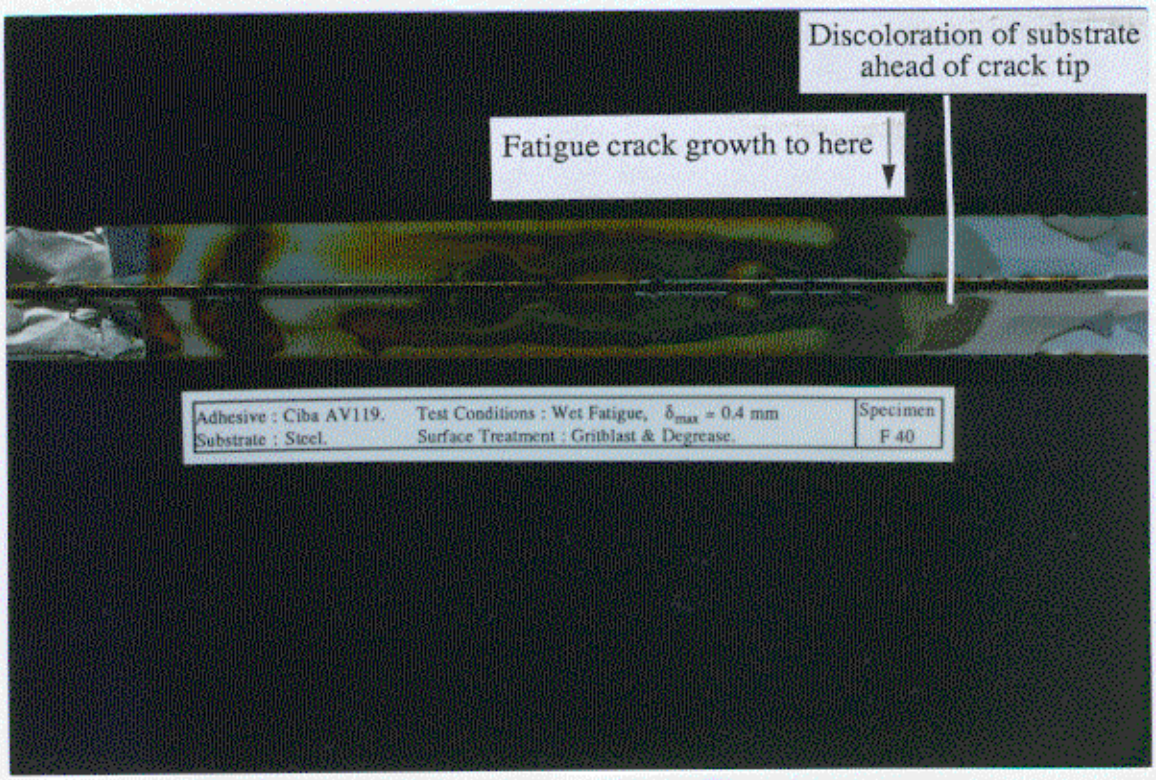

Figure 18. **Fracture surface of steel specimen bonded with 'AV119', tested 'wet', showing areas of cohesive-in-adhesive failure (cream) and discoloration ahead of crack tip.**

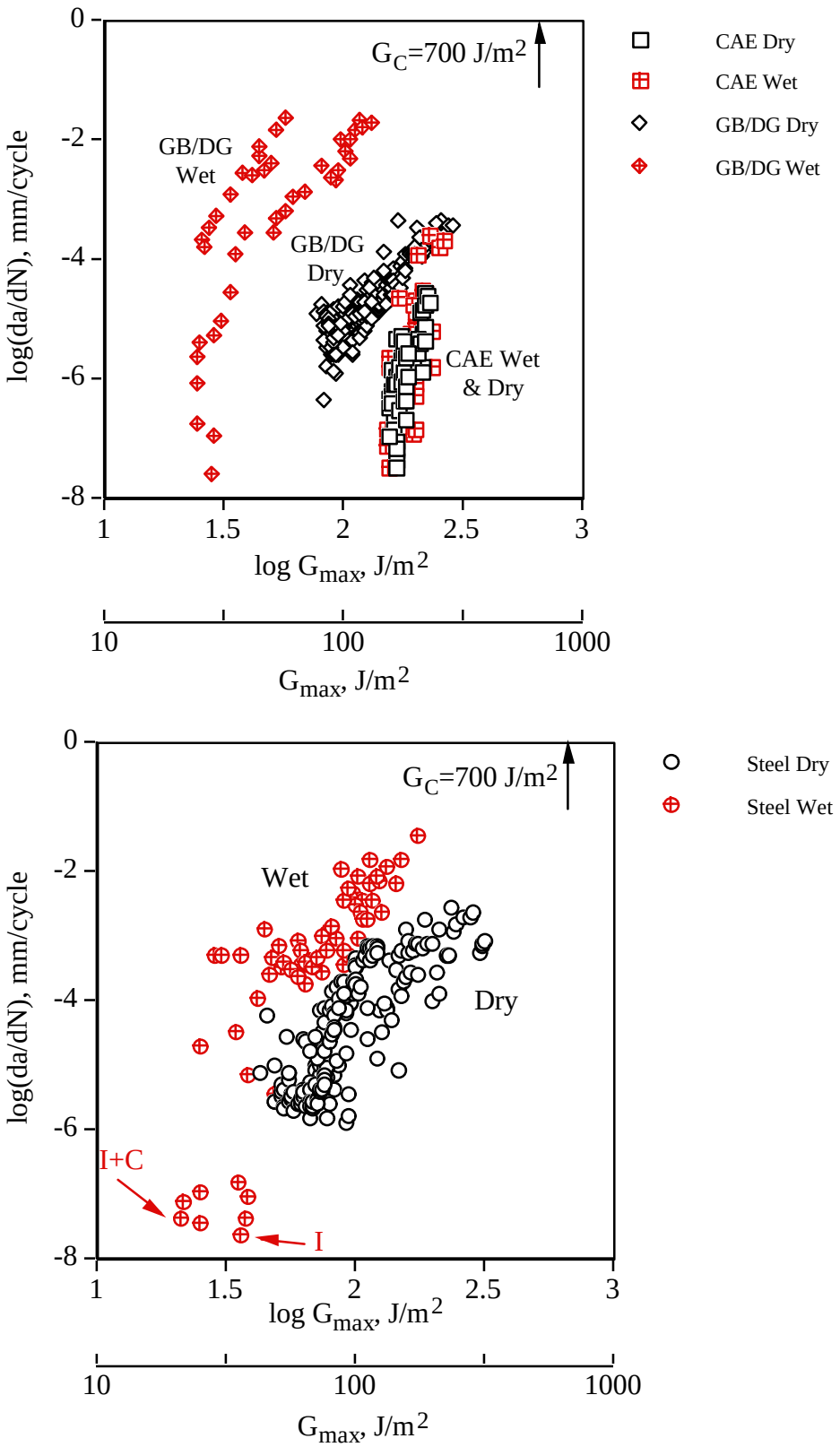

Figure 19. Rate of crack growth versus applied maximum fracture energy for 'AV119' adhesive, (a) Aluminium substrates, chromic-acid etch and gritblast/degrease surface treatments, (b) Steel substrates.

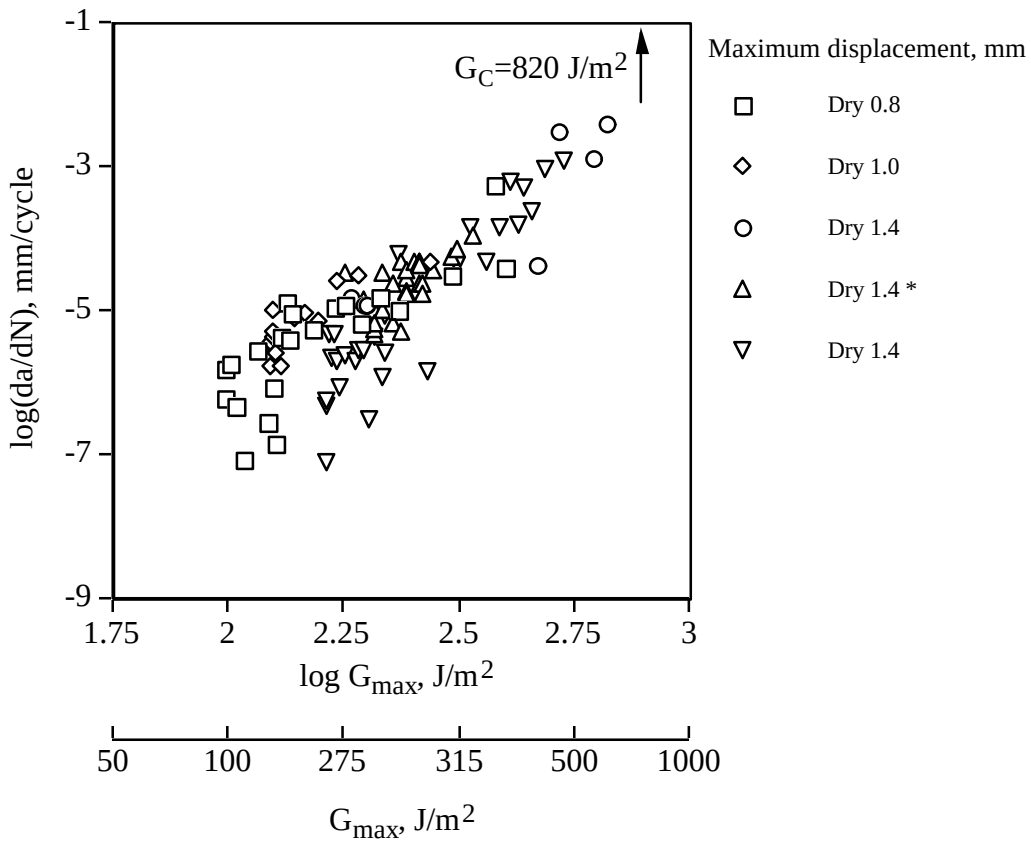

Figure 20. Rate of crack growth versus applied maximum fracture energy for 'F241' adhesive with chromic-acid etched aluminium substrates, (a) 'Dry', (b) 'Wet'.

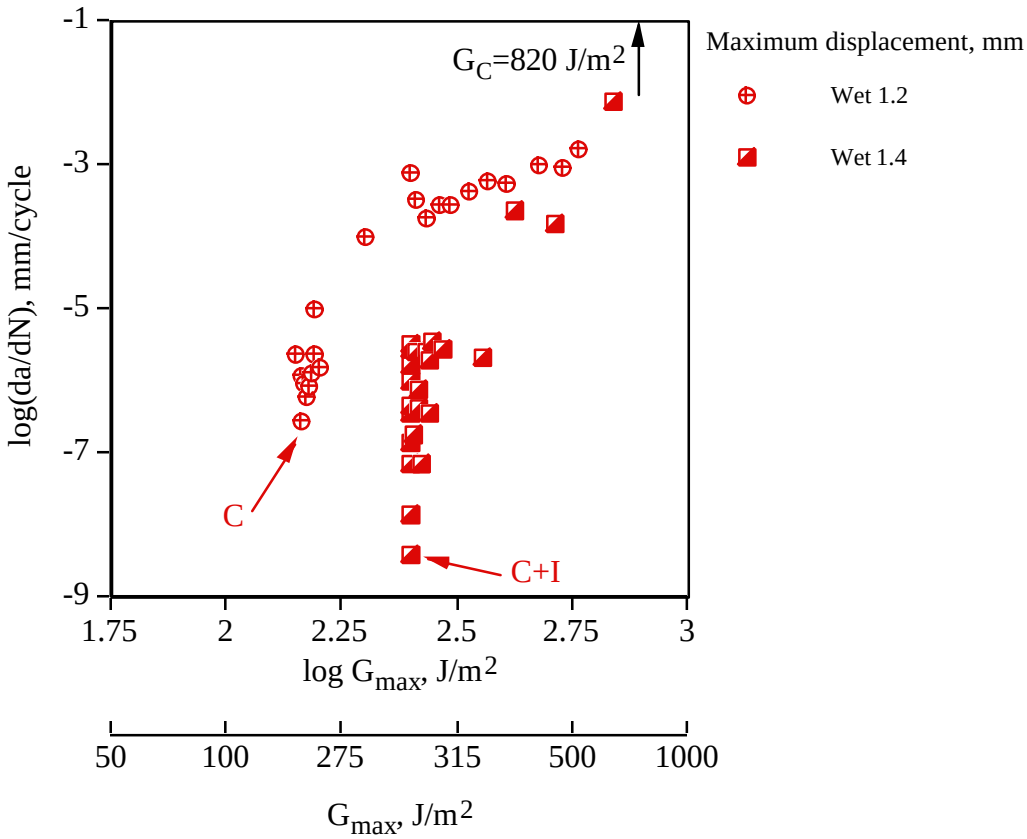

Figure 20. **Rate of crack growth versus applied maximum fracture energy for 'F241' adhesive with chromic-acid etched aluminium substrates, (a) 'Dry', (b) 'Wet'.**

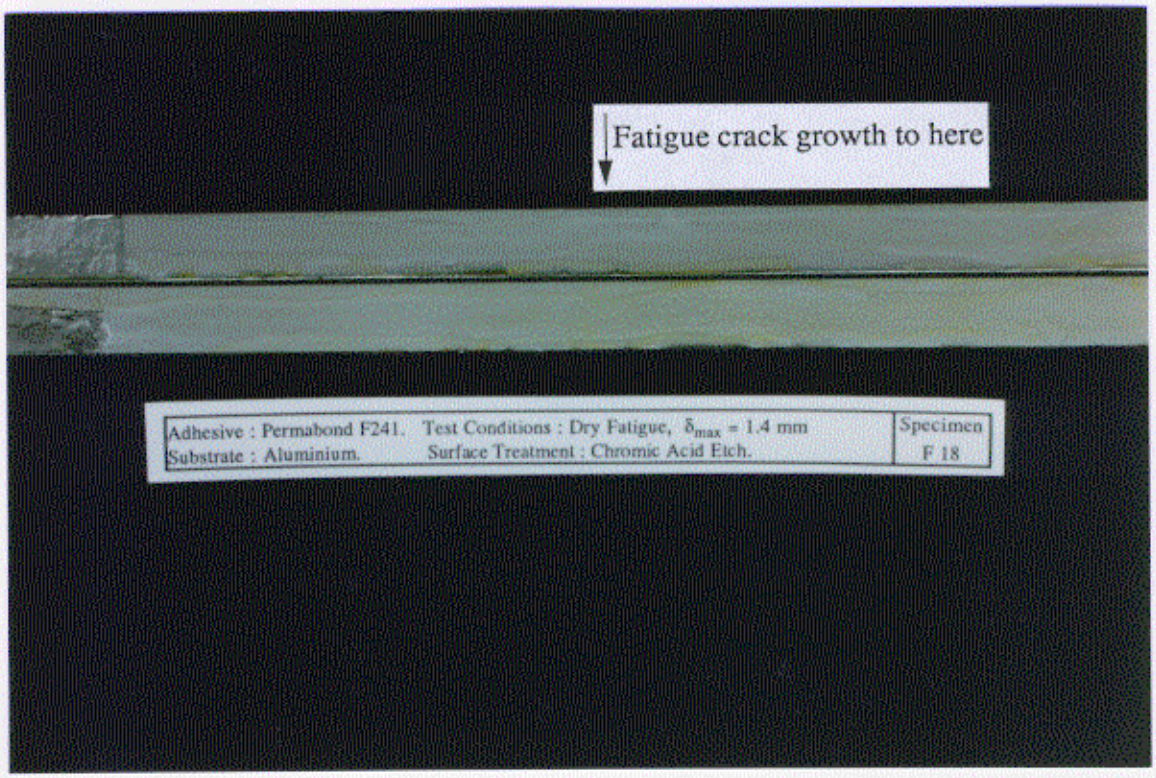

Figure 21. **Fracture surface of chromic-acid etched aluminium specimen bonded with 'F241', tested 'dry' showing cohesive-in-adhesive failure.**

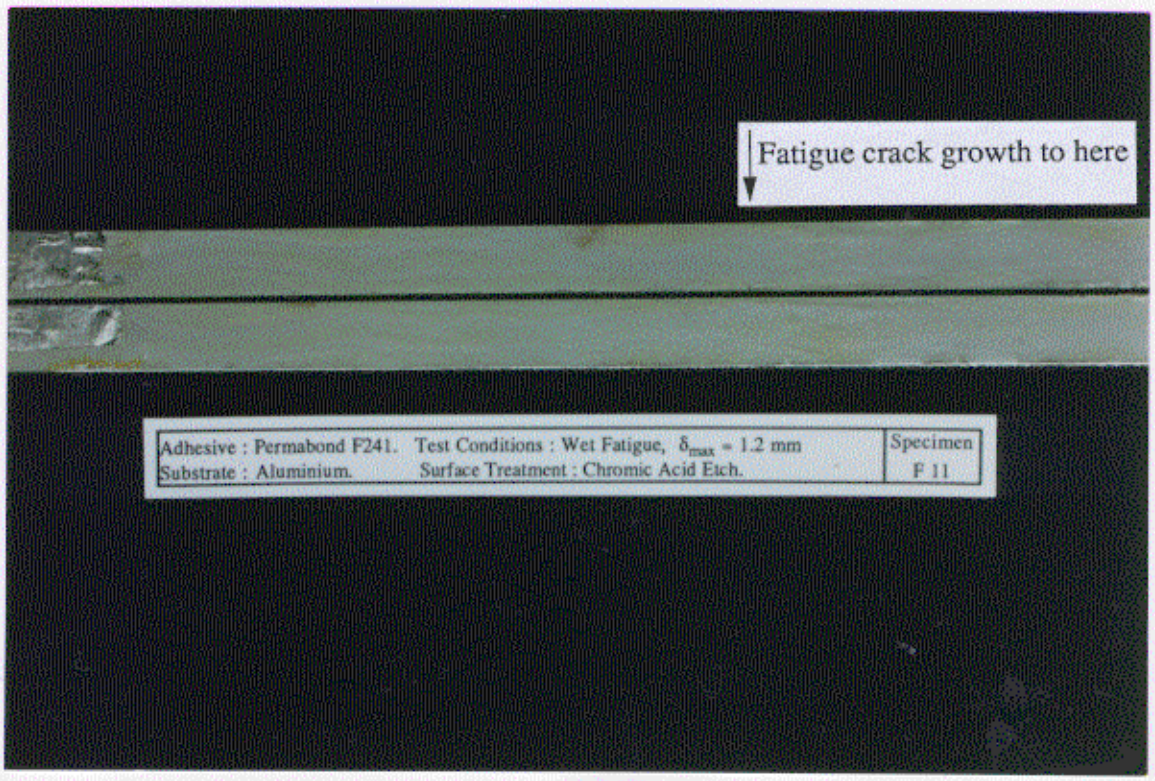

Figure 22. **Fracture surface of CAE aluminium specimen bonded with 'F241', tested 'wet', showing cohesive-in-adhesive failure.**

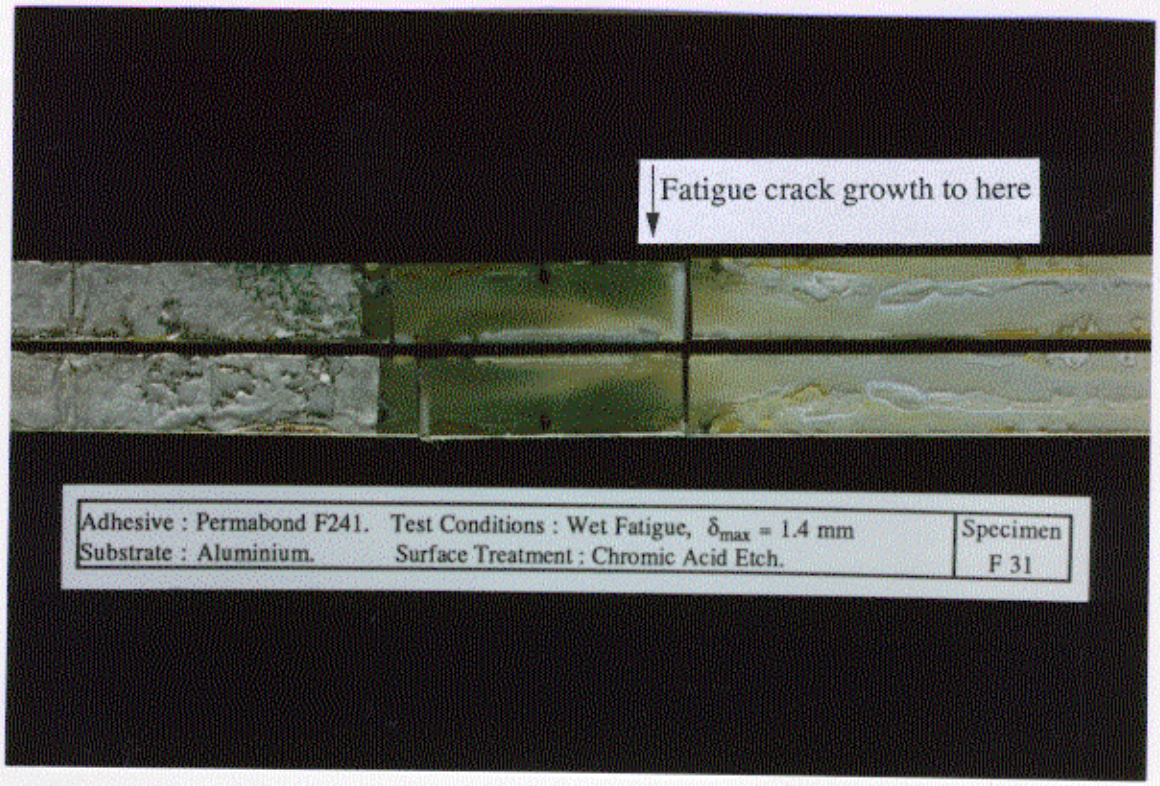

a) Specimen photograph.

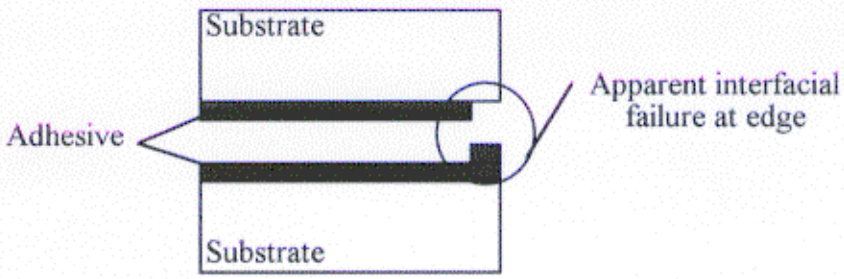

b) Cross-section showing apparently interfacial failure at edge.

Figure 23. Fracture surface of CAE aluminium specimen bonded with 'F241', tested 'wet', showing discoloration of adhesive and apparently interfacial failure at edge of specimen, (a) Specimen photograph, (b) Cross-section.

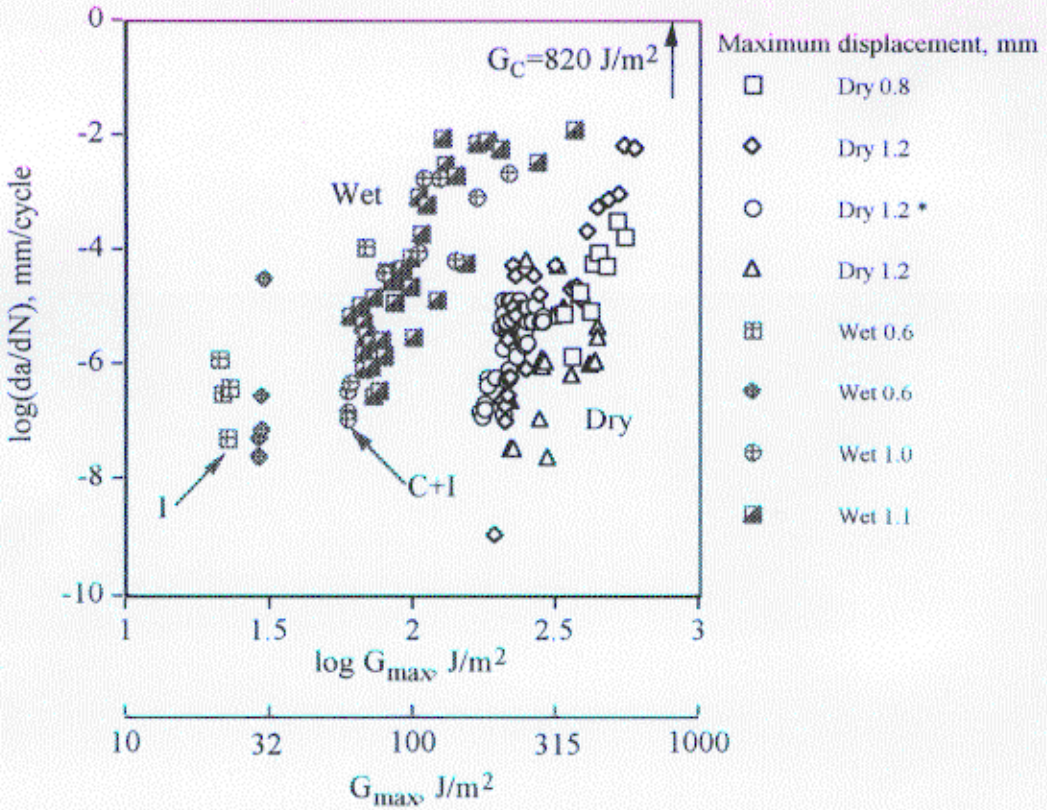

Figure 24. **Rate of crack growth versus applied maximum fracture energy for 'F241' adhesive with aluminium substrates, gritblast/degrease surface treatment, (* denotes crack gauge data).**

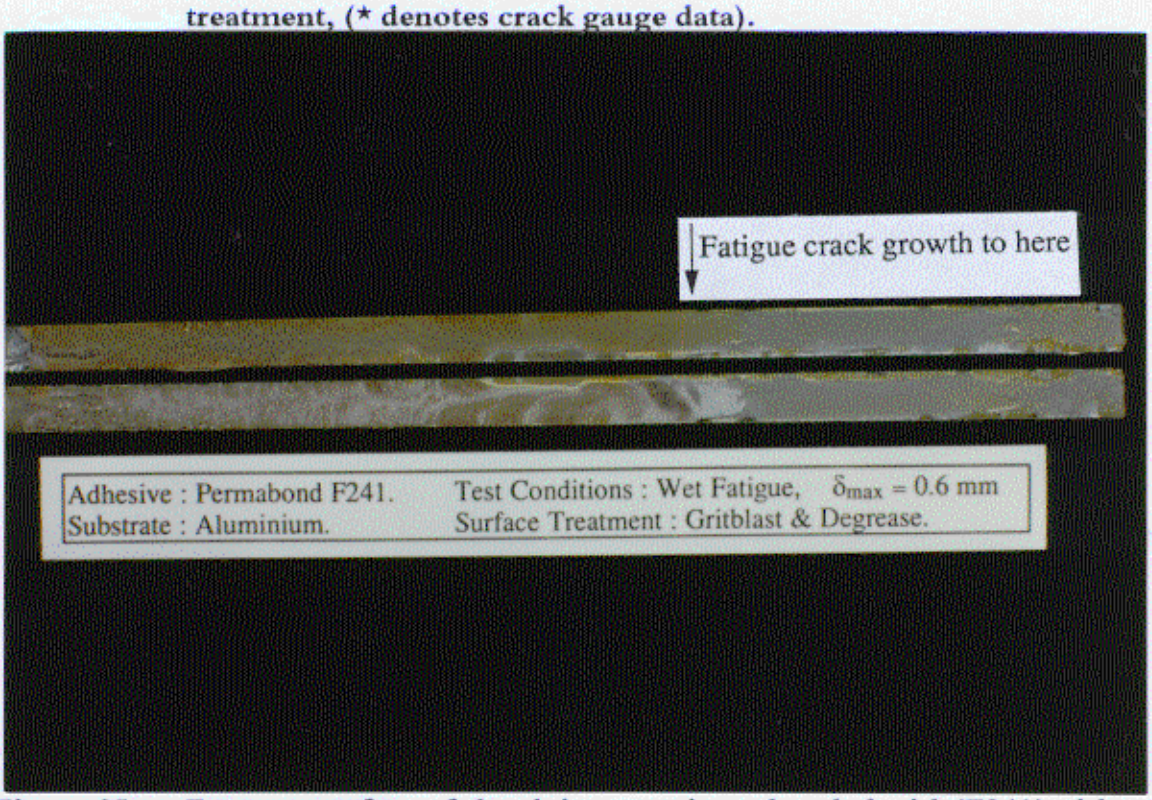

Figure 25. **Fracture surface of aluminium specimen bonded with 'F241' with GB/DG surface treatment, tested 'wet', showing apparently interfacial failure.**

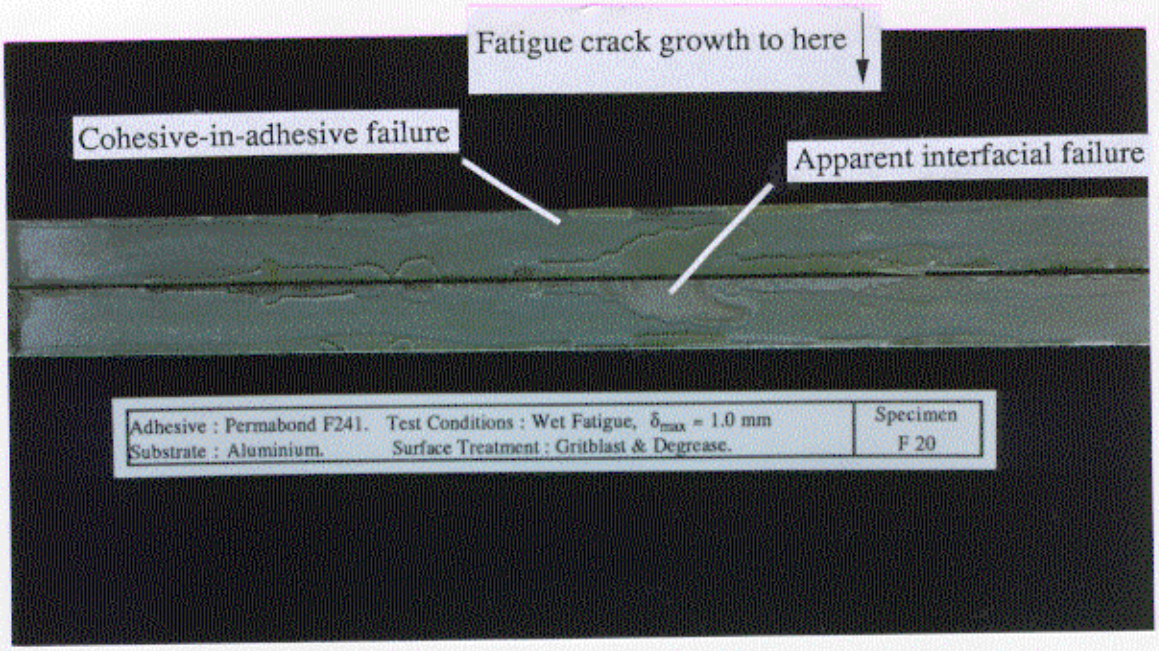

Figure 26. **Fracture surface of aluminium specimen bonded with 'F241' with GB/DG surface treatment, tested 'wet', showing areas of cohesive-in-adhesive and apparently interfacial failure.**

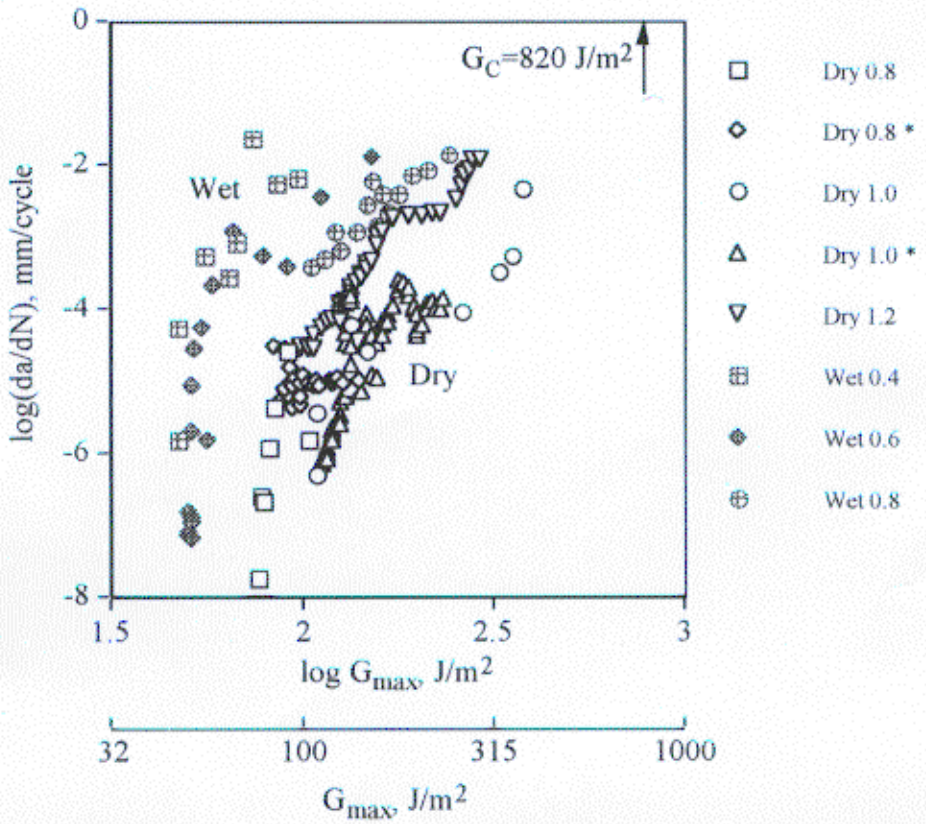

Figure 27. **Rate of crack growth versus applied maximum fracture energy for 'F241' adhesive on steel substrates, (* denotes crack gauge data, otherwise by travelling microscope).**

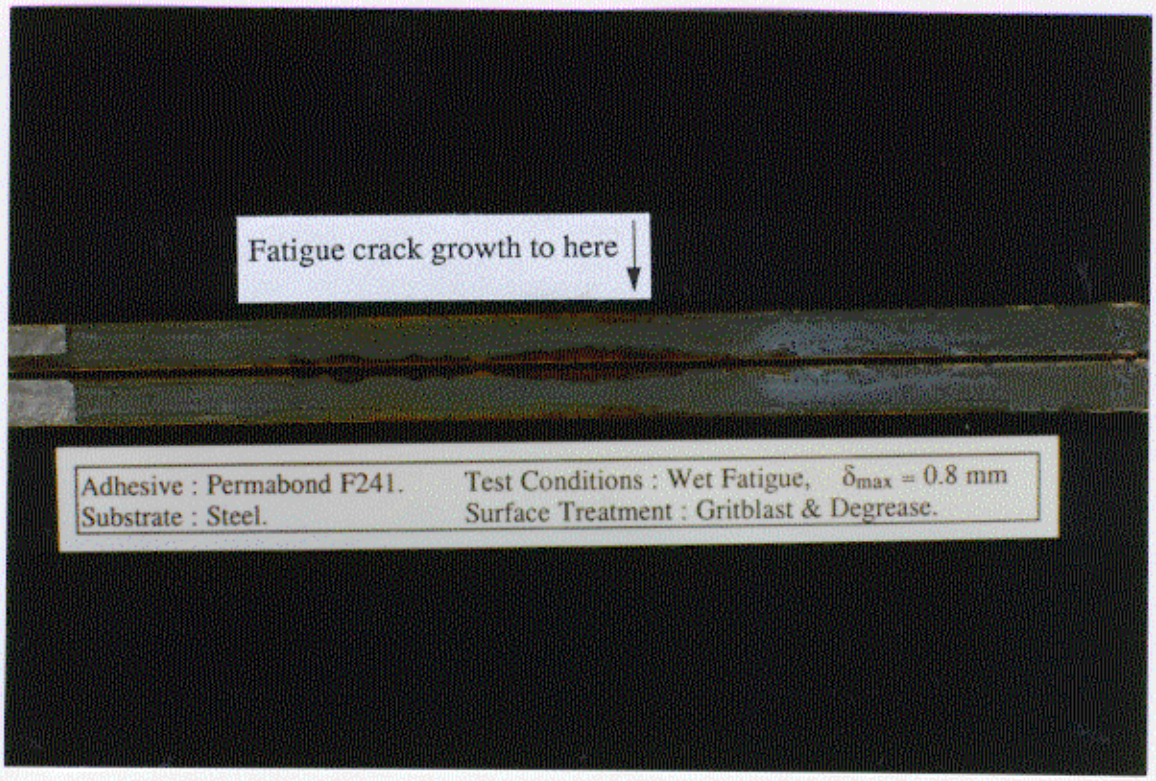

Figure 28. **Fracture surface of 'F241'/steel specimen, tested 'wet' showing cohesive-in-adhesive failure along centre of specimen (grey areas) and apparently interfacial failure along edge with corrosion of exposed substrate (brown areas). Note both halves of specimen are corroded indicating failure within oxide layer.**

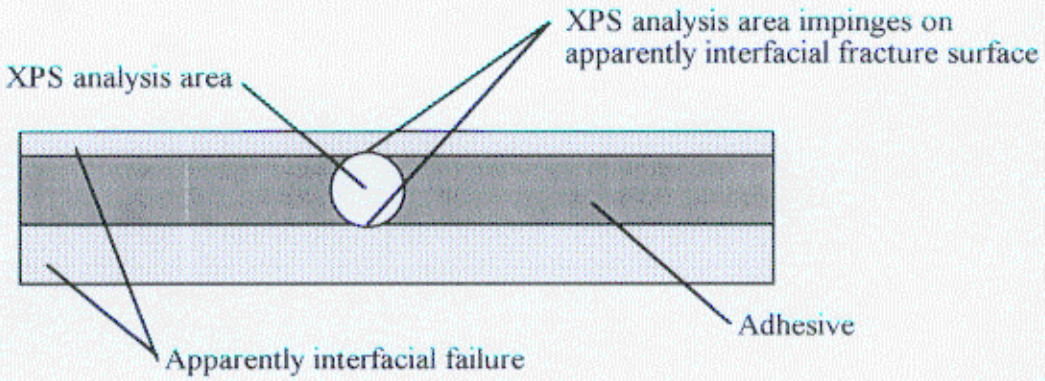

Figure 29. **Plan view of XPS analysis area on 'F241'/steel specimens tested 'wet', as shown above in Figure 28. Note that the XPS data, shown in Table 11, will include some data from the apparently interfacial failure.**

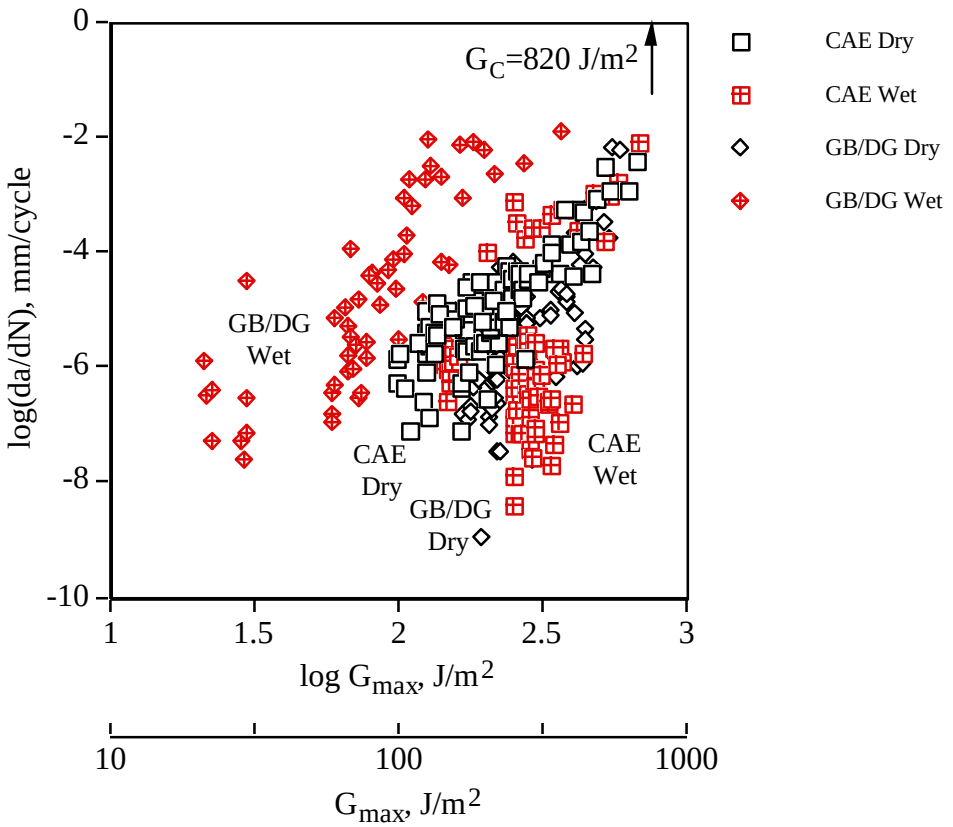

Figure 30. **Rate of crack growth versus applied maximum fracture energy for 'F241' adhesive with aluminium substrates, chromic-acid etch and gritblast/degrease surface treatments.**

6 Single Lap Joints

6.1 INTRODUCTION

The single lap joint, as shown in Figure 31, is a very common joint design. It is frequently used to compare the performance of adhesive joints under fatigue loading[16]. 'AV119'/steel joints were tested immersed in water to provide experimental data for comparison with the lifetimes that can be predicted from the fracture mechanics data obtained in section 5. The lifetime prediction model will be discussed in section 7.

6.2 SPECIMEN MANUFACTURE

The lap joint specimens were made using the method laid down in the ASTM Standard[17]. Sheets of 2 mm thick steel were milled to size, approximately 250 by 100 mm. The area to be bonded was degreased with acetone, gritblasted and degreased again. Adhesive was applied and spread to approximately 15 mm from the edge of the sheet. Stainless steel wire spacers were placed at either end and in the middle of the strip. The sheets were placed in a jig to ensure that they were parallel, with an overlap length of 12.7 mm. Pressure was applied using an aluminium bar and 5 lb masses. The joints were cured at 120°C for 2 hours.

After curing, the sheets were cut into 25.4 mm wide specimens, discarding the edge and centre sections.

6.3 EXPERIMENTAL PROCEDURE

6.3.1 Static

Before testing the width of the bonded region and the overlap length were measured, and the bonded area calculated. Specimens were tested on a screw-driven Instron testing machine. Spacers were used to ensure that the arms of the joint were parallel to the loading direction. The grips were attached to the testing machine using universal joints to eliminate any misalignment. A grip separation of 140 mm was used, as recommended by the ASTM Standard[17]. A crosshead speed of 0.5 mm/min was used. The maximum load was recorded, and the nominal failure stress calculated by dividing the load by the bonded area. Two specimens were tested from each sheet.

6.3.2 Fatigue

Joints were tested on a Mand servo-hydraulic testing machine using the same fixtures as for the static testing. Tests were conducted under load control using a load ratio (P_{min}/P_{max}) of 0.5, with a sinusoidal loading waveform. Maximum nominal stresses from 30 to 90 % of the static value were used. The number of cycles to failure was recorded.

Tests were conducted 'wet', with the joint immersed in distilled water. A small tank was used, see Figure 32, with a tapered silicone rubber bung which sealed around one arm of the specimen when compressed. The tank rested on the lower grip of the testing machine. The water circulator heaters used for the TDCB tests gave too high a flow rate for this tank, so a peristaltic pump was used to circulate water into the tank, with a gravity-fed return to the

reservoir, see Figure 33. This enabled a constant 28°C water temperature to be maintained around the lap joint.

6.4 RESULTS

6.4.1 Static

The tests gave a mean nominal failure stress of 24 MN/m^2, with a standard deviation of 2.3 MN/m^2. Failure loads were in the order of 7700 N. Failure was apparently interfacial, see Figure 34. Areas of adhesive that had failed close to both interfaces were present, i.e. leaving a flap of adhesive that was detached from both substrates, as shown in Figure 34 as area 4 on the 'metal' side of the joint.

6.4.2 Fatigue

The single lap joint fatigue results are shown in Figure 35. At high stress levels the joint life is short. Even at 60 % of the static failure stress, the joint life is less than 10000 cycles, see Figure 36. This is equivalent to half an hour at 5 Hz. Joint lives of over 24 hours are seen at below 35 % of the static stress. Joint life increases rapidly at around 30 % of the static stress, where it could exceed 14 x 10^6 cycles. This is evidence of an effective threshold, see Figure 35, below which failure does not occur, as indicated by previous work[14,16.]

The joints exhibited mostly apparently interfacial failure, as shown in Figure 37. The same locus of failure was seen with the TDCB specimens. Corrosion was present on the fracture surfaces of the joints tested at lower applied stress levels. It is unlikely that all the corrosion occurred post-failure as joints were removed from the water soon after failure. This is further evidence of crack growth for a significant proportion of the fatigue life.

Surface analyses were performed on specimens with AES and XPS, as shown in Table 13. The results show surface contamination by silicon, probably due to decomposition of the silicone rubber bung used to seal around the specimen, see Figure 32. However though no iron is detected at zero depth on the fracture surfaces, over 25 % is detected at a depth of 10 nm. Area 1 on the metal side shows both iron and carbon at a depth of 10 nm, as does the counterface on the adhesive side. This would indicate that the failure is through the iron oxide, with residual adhesive. The persistent presence of carbon in the depth profile of the 'dark' area shows that there is a thicker layer of residual adhesive than in the 'light' area. However, failure is still through the iron oxide. The same locus of failure was seen with the steel TDCB specimens bonded with the 'AV119' adhesive when tested wet.

The increasing ratio of iron to oxygen with depth shows that the proportion of elemental iron is increasing with depth. At a depth of 20 nm there is a significant amount of elemental iron plus some oxide present. Thus the oxide layer is relatively thin.

6.5 BACKFACE STRAIN

6.5.1 Introduction

A backface strain technique was used to investigate crack growth in the lap joints under fatigue. Work by Zhang et al[18] and Imanaka et al[19] has shown that it is possible to detect crack growth using strain gauges bonded on the backface of the specimen, opposite the end of the overlap, Figure 38a. Loading the specimen puts both gauges into compression, Figure 38b. Softening of the adhesive causes the backface strain to become less compressive. When a crack starts to grow

from one end of the overlap the local deformation relaxes, and the compression on one gauge is decreased, but increased on the other, Figure 38c. Crack growth from the other end of the overlap will cause a compression decrease in both gauges, Figure 38d.

The best results are obtained when the gauges are as small as possible as a crack can be detected when it is half as long as the gauge. Imanaka et al[19] positioned the gauges centrally above the end of the overlap. However, the sensitivity of the technique can be improved by offsetting the gauges towards the ends of the specimen[18]. The gauges used in the current work had a grid size of 1.57 mm square. According to Zhang et al[18] the crack will be detected when it is approximately 0.8 mm long.

6.5.2 Experimental Procedure

Strain gauges were attached to the specimens using the same bonding procedure as used for the crack propagation gauges, see section 5.4.2 above. The gauges were connected to an amplifier, and all the wires and connections sealed with polyurethane varnish to prevent the water immersion causing a short circuit. The signal from the gauges was sampled by computer, via the 'MacLab'. The load and displacement outputs from the testing machine were also recorded. A one second sample was taken every minute. This produced a large amount of data, but the high sampling frequency was required as the measured strain increased rapidly near final failure.

The data was analysed to provide values of maximum load and minimum strain (strains are negative) against the number of cycles.

6.5.3 Backface Strain Results

The backface strain technique has shown crack growth for much of the fatigue life of the single lap joints. An example result is shown in Figure 39. The gaps between the data points occur where the data logger stopped recording and had to be re-started.

In Figure 39, the initial compressive strain decreases, i.e. becomes more tensile, as plasticisation affects the adhesive. A crack is detected after about 3.5×10^6 cycles, when the compressive strain from gauge B increases. Further crack growth is indicated by the continued increase in the compressive strain measured by gauge B while the strain in gauge A decreases. Thus, there has been crack growth for over 75 % of the joint life, perhaps more as the joint had not failed when the test was stopped after 14×10^6 cycles. Other tests showed crack growth for over 85 % of the joint life.

The slope of the strain versus cycles graph increased rapidly close to final failure. This indicates that the crack growth rate increases, as the FE work by Zhang et al[18] shows a linear relationship between crack length and backface strain.

The backface strain work by Zhang et al[18] on single lap joints has also shown that crack growth accounts for between 40 and 70 % of the fatigue life. This confirms observations that crack propagation accounts for much of the fatigue life made using ultrasonic techniques on other lap joint specimens[21], but contradicts other earlier research[16].

6.6 CONCLUSIONS

The static testing gave a nominal failure stress for 'dry' 'AV119'/steel joints of 24 MN/m^2. 'Wet' fatigue testing showed short lives at high applied stress levels (less than 10000 cycles down to

60 % of the static failure stress). The joint life increased with decreasing applied stress. Evidence of a threshold at around 30 % was indicated by fatigue lives over 14 x 10^6 cycles. The use of a backface strain technique showed crack growth for over 75 % of the life of the lap joints.

	Area	**Depth, nm**	**Fe**	**Si**	**C**	**O**
'Metal' Side	(Light) 1	0	0	50.1	25.4	24.5
		5	10.8	42.8	18.1	28.2
		10	26.9	31.0	12.7	29.4
		20	63.6	0	11.2	25.1
'Metal' Side	(Dark) 3	0	0	35.4	21.5	43.0
		5	0	24.5	34.6	40.9
		10	32.8	14.9	27.5	24.8
		20	35.6	3.4	40.2	20.8
		30	37.7	0	45.0	17.3
		50	44.6	0	40.0	15.4
		100	49.8	0	38.8	11.4
'Adhesive' Side	General	0	0	37.7	32.8	29.5
		10	26.7	3.1	21.6	48.6
		20	24.5	0	30.4	45.1

a) AES analysis.

Note
1. See Figure 37 for identification of analysis areas.

	Depth, nm	**Fe**	**Si**	**C**	**N**	**O**
'Adhesive'	0	0	13.7	62.2	2.5	21.6

b) XPS analysis.

Table 13. Surface analysis results for 'AV119'/steel lap joint specimen tested in 'wet' fatigue, also see Figure 33.

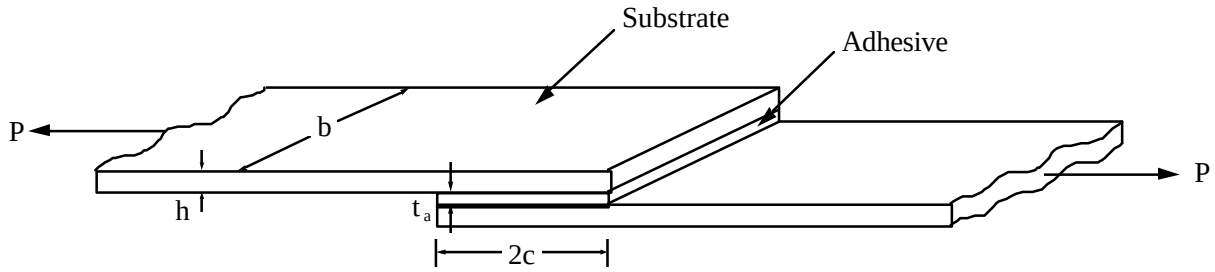

Figure 31. The single lap joint.

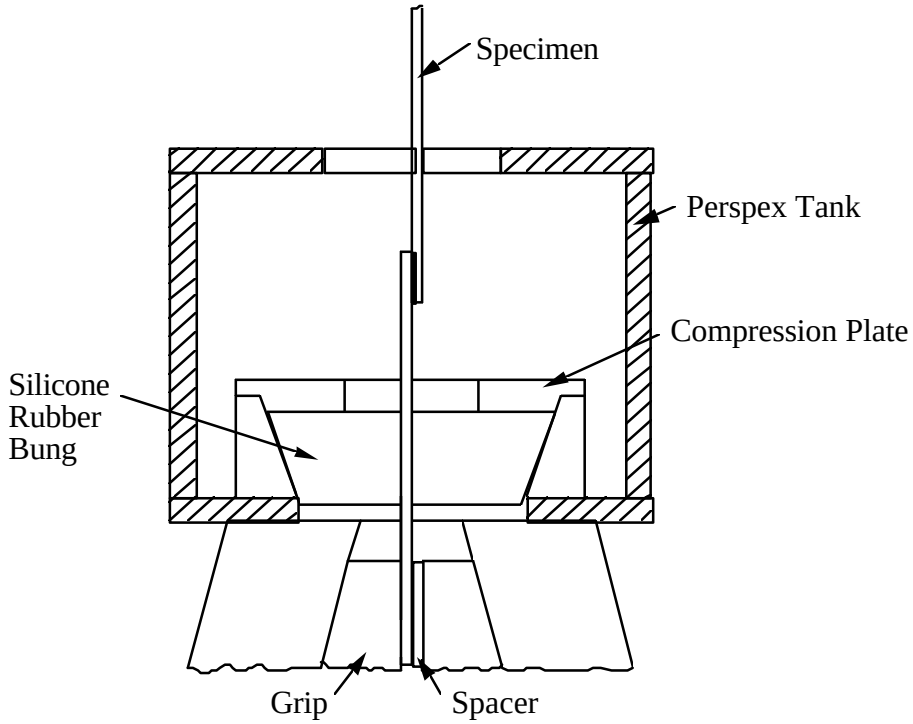

Figure 32. Water tank used for lap joint tests.

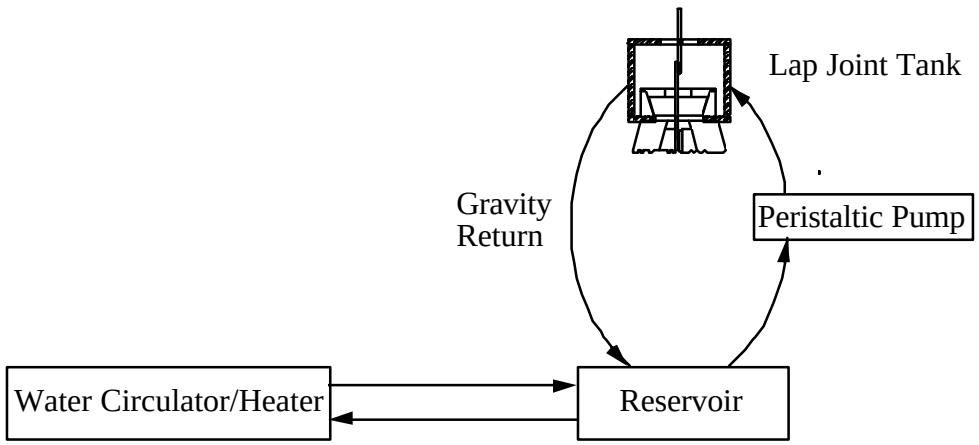

Figure 33. Schematic of water circulation system for lap joint tests.

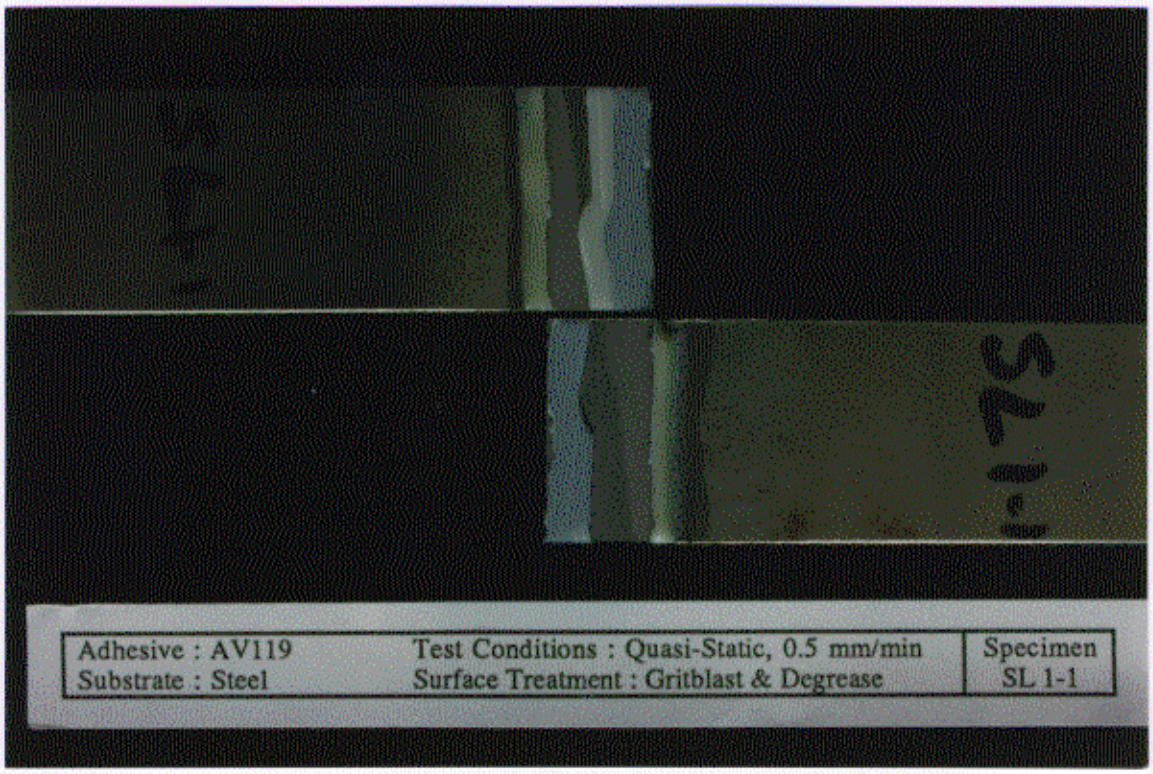

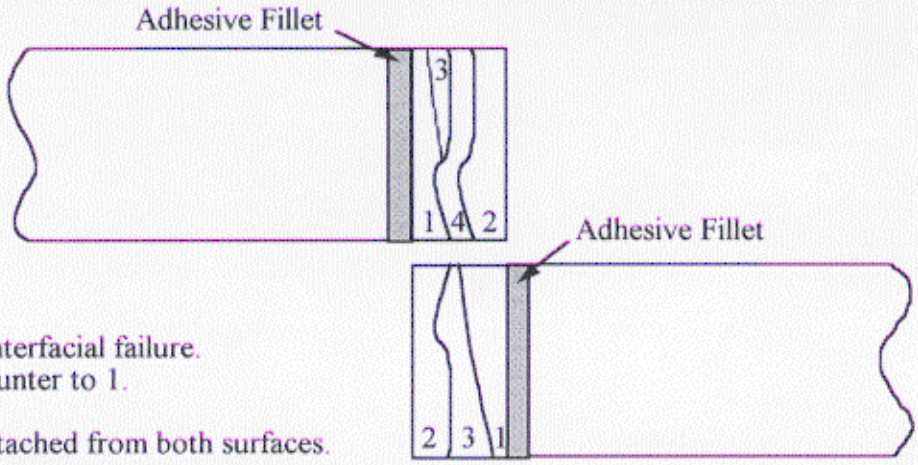

Key:
1. Apparently interfacial failure.
2. Adhesive, counter to 1.
3. Adhesive.
4. Adhesive, detached from both surfaces.

Figure 34. **(a) Fracture surface of 'AV119'/steel lap joint specimen after static testing, with (b) identification of areas of failure surface.**

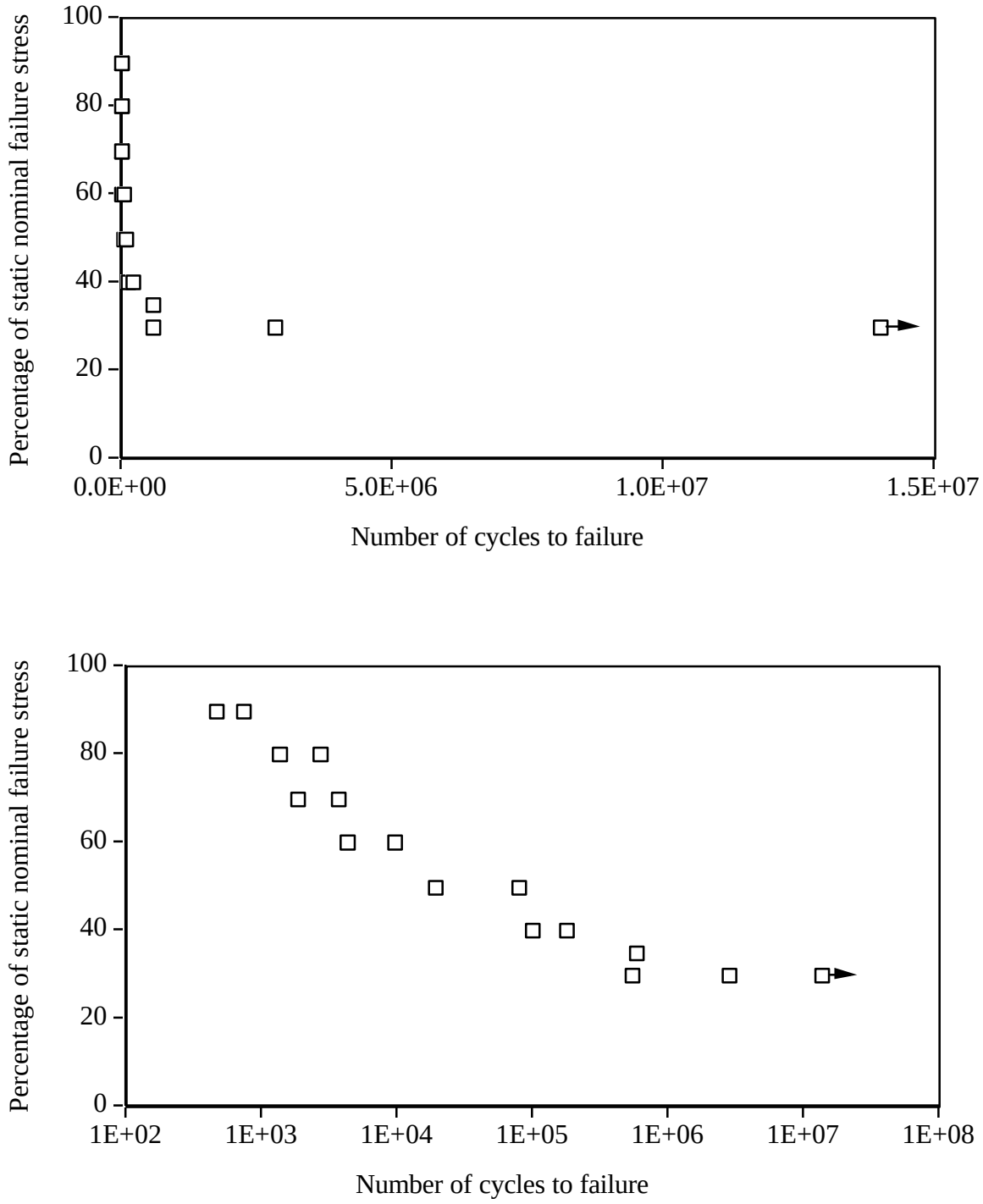

Figure 35. Percentage of static failure stress versus fatigue life for 'AV119'/steel lap joints tested 'wet', (a) linear axis, (b) logarithmic axis.

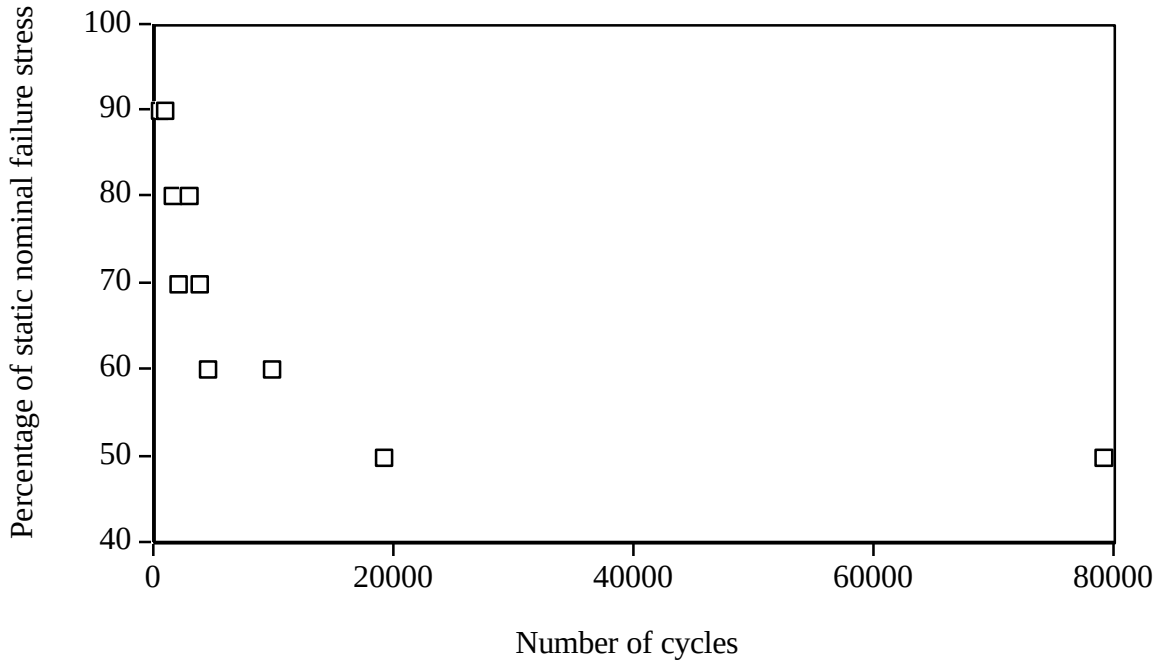

Figure 36. Fatigue life of 'wet' 'AV119'/steel lap joints for stress levels above 50 % of static.

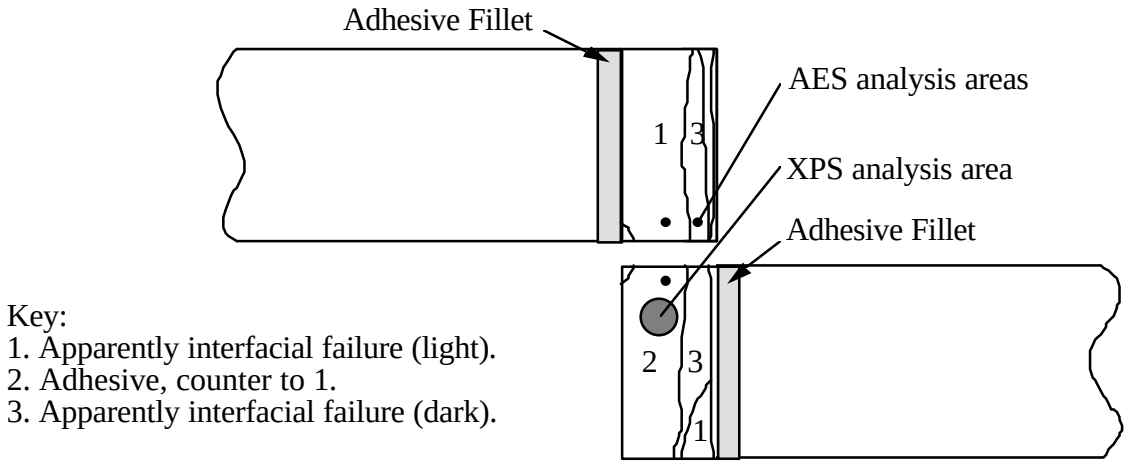

Figure 37. Fracture surface of lap joint after fatigue testing, showing apparently interfacial failure. Maximum applied stress of 70 % of static. See Table 13 for surface analysis results.

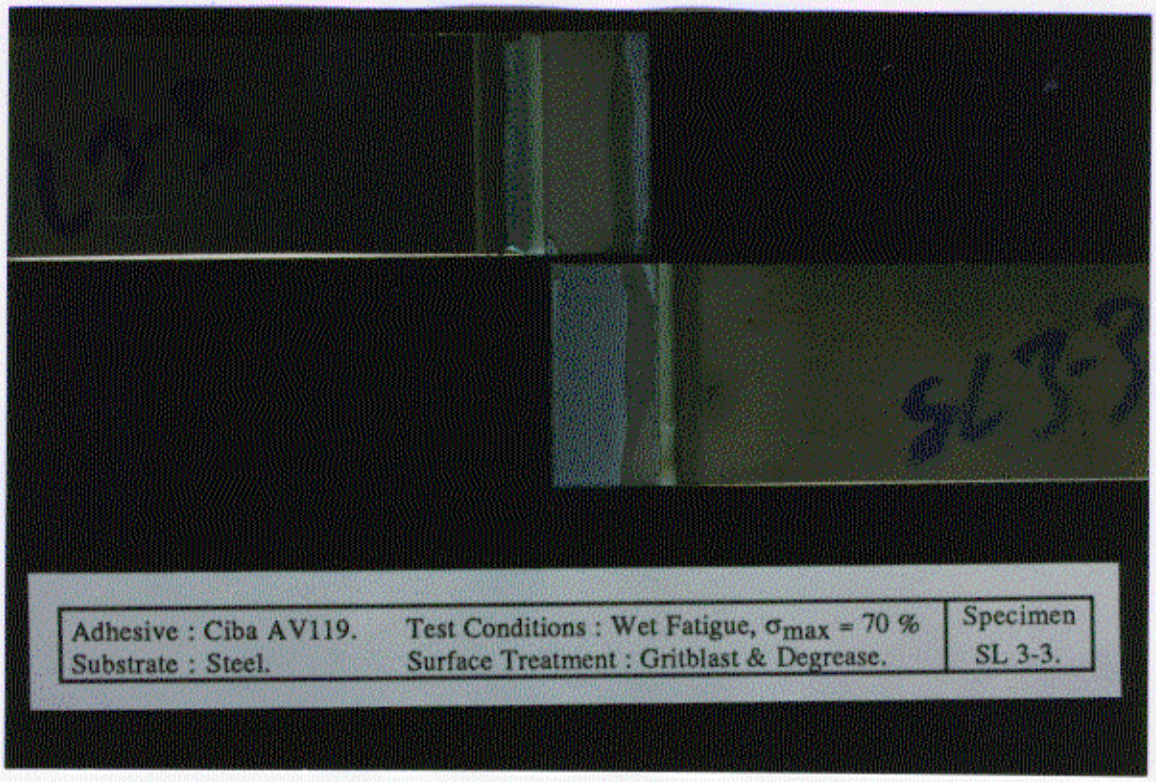

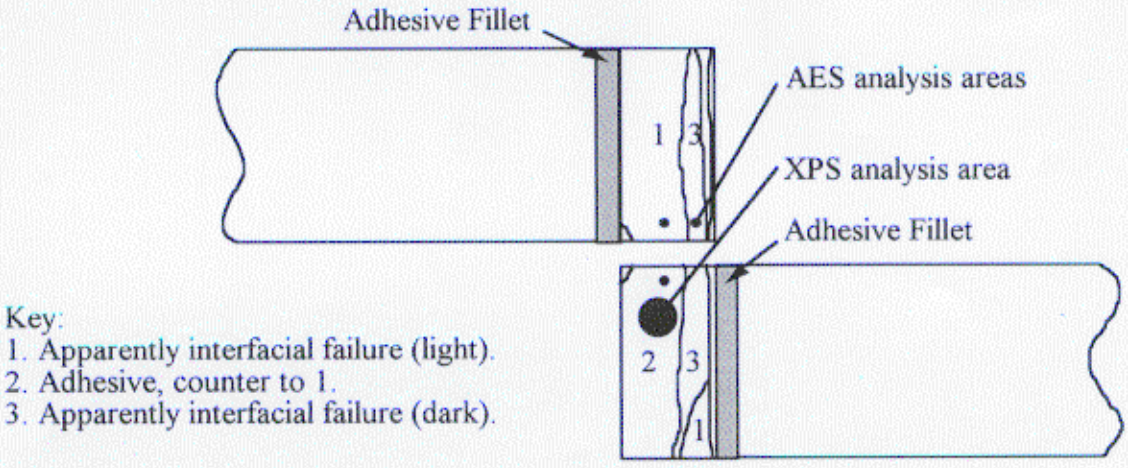

Key:
1. Apparently interfacial failure (light).
2. Adhesive, counter to 1.
3. Apparently interfacial failure (dark).

Figure 37. **Fracture surface of lap joint after fatigue testing, showing apparently interfacial failure. Maximum applied stress of 70 % of static. See Table 13 for surface analysis results.**

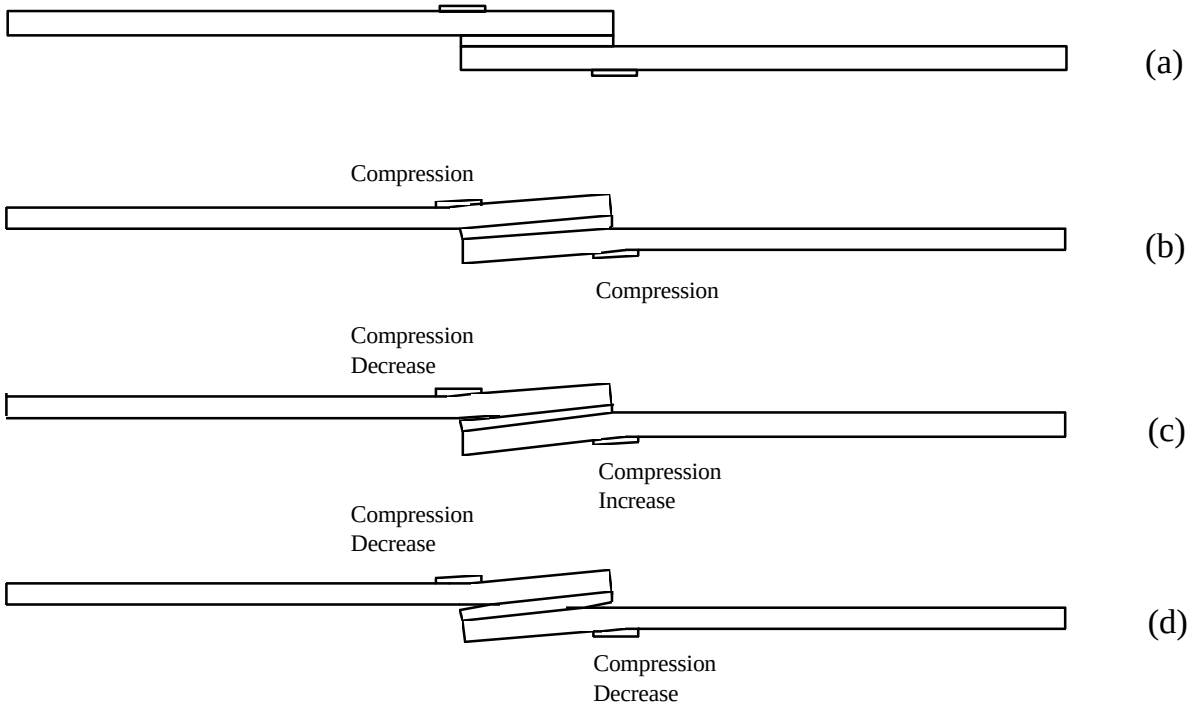

Figure 38. The backface strain technique, showing effect of crack growth on measured strain.

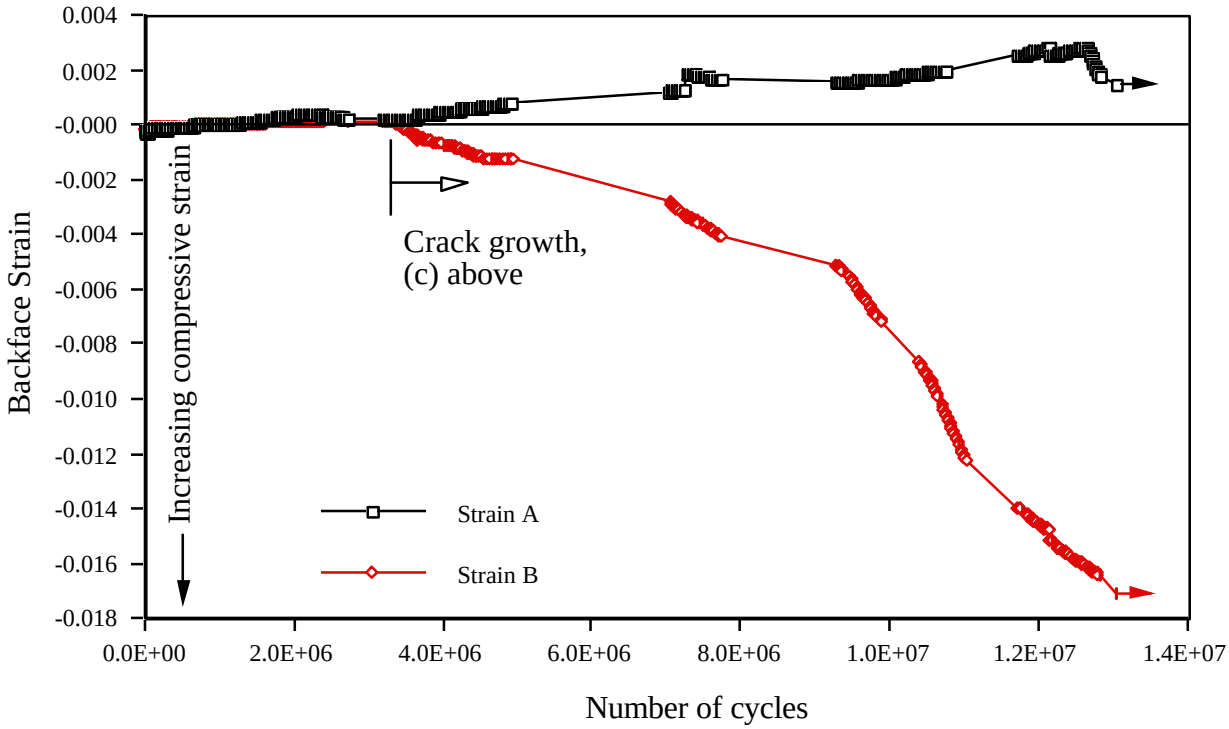

Figure 39. Backface strain versus number of cycles for lap joint. Crack growth is identified after 3.5 x 10^6 cycles, but at 14 x 10^6 cycles joint failure has not yet occured.

7 Lifetime Predictions

7.1 INTRODUCTION

Previous work by Kinloch & Osiyemi[21] has shown that it is possible to predict the life of lap joints in fatigue using data from adhesively-bonded composite double-cantilever beam tests. These were tested 'dry' under fatigue loading by the authors. This work was extended to adhesively bonded aluminium specimens using data generated from 'dry' TDCB tests[14,20]. The intention is to apply this method to steel joints in a 'wet' environment using data generated by the TDCB tests discussed in section 5.

7.2 ANALYSIS

The analysis used by Kinloch & Osiyemi[21] is equally applicable to the bonded metal joints used here. The data required is the solution to Equation 11.

To predict the lifetime, it is necessary to find the strain energy release rate for a single lap joint, see Figure 31. It has been shown that these joints fail due to transverse tensile (s_{11}) stresses. The maximum value of this cleavage stress can be found from analyses by Hart-Smith[22] and Zhao et al[23]:

$$s_{11} = M_e \left(\frac{E_a}{2 t_a X} \right)^{1/2} \qquad (12)$$

where E_a and t_a are the modulus and thickness of the adhesive. The bending stiffness, X, is given by:

$$X = \frac{E_s h^3}{12 \left(1 - u^2\right)} \qquad (13)$$

where E_S, h and υ are the modulus, thickness and Poisson's ratio of the substrate.

The bending moment per unit width, M_e, can be found from:

$$M_e = 0.5 KT \left(h + t_a\right) \qquad (14)$$

where K, the bending moment factor, is given by:

$$K = \frac{1}{1 + ec} \qquad (15)$$

where c is the overlap length of the joint, and

$$e = \left(\frac{T}{X}\right)^{1/2} \tag{16}$$

Here T is the load per unit width applied to the joint.

The strain energy release rate in a cracked beam can be found from work by Williams[23], given a knowledge of the bending moments at the crack tip. For mode I this analysis gives:

$$G = \frac{12\,M_e^2}{E_s h^3} \tag{17}$$

This assumes symmetrical loading of the joint. Substituting Equation 14 into Equation 17, and using Equations 15 and 16, gives an expression for G_{max}:

$$G_{max} = \frac{12}{E_s h^3}\left(\frac{T_{max}\left(h+t_a\right)}{2}\right)^2\left(\frac{1}{\left(1+ec\right)^2}\right) \tag{18}$$

where T_{max} is the maximum load applied to the lap joint in a fatigue cycle (per unit joint width).

Assuming that a crack will grow through the adhesive layer parallel to the loading direction, then if it grows by a length a from both ends of the lap joint, the effective overlap length will be reduced from 2c to (2c-2a). Substituting this into Equation 18 gives:

$$G_{max} = \frac{12}{E_s h^3}\left(\frac{T_{max}\left(h+t_a\right)}{2}\right)^2\left(\frac{1}{\left(1+e[c-a]\right)^2}\right) \tag{19}$$

Combining Equations 11 and 19, eliminating G_{max}, gives an integral expression for the expected number of cycles to failure of the lap joint:

$$N_f = \int_{a_o}^{a_f} \frac{\left[E_s h^3\left[1+e(c-a)\right]^2\right]^{-n_2}}{D G_c^{n_2}\left[3\left[T_{max}\left(h+t_a\right)\right]^2\right]^{n-n_1}} \cdot \left[\frac{\left[G_c E_s h^3\left[1+e(c-a)\right]^2\right]^{n_2} - \left[3\left[T_{max}\left(h+t_a\right)\right]^2\right]^{n_2}}{\left[3\left[T_{max}\left(h+t_a\right)\right]^2\right]^{n_1} - \left[G_{th} E_s h^3\left[1+e(c-a)\right]^2\right]^{n_1}}\right] \tag{20}$$

The integration limits are the initial flaw size, a_O, and the final crack length, a_f, where rapid crack growth and failure occurs.

From the TDCB testing, the values of D, n, n_1, n_2, G_{th} and G_C are known. The geometry of the lap joint and the material properties of the substrate give e, h, t_a, c and E_S. Thus if expressions for a_O and a_f can be found, then we can predict N_f for a given maximum load per unit width.

Fracture mechanics can be used to find a_o, from the Griffith Equation:

$$a_o = \frac{E_a G_c}{\pi \sigma_a^2} \qquad (21)$$

where s_a is the tensile strength of the adhesive.

Rearranging Equation 19, putting G_{max} equal to G_C, gives the crack length at failure. This is a_f:

$$a_f = c - \frac{1}{e}\left[\left(\frac{3\left(T_{\max}\left[h + t_a\right]\right)^2}{E_s h^3 G_c}\right)^{1/2} - 1\right] \qquad (22)$$

Thus we now have an equation to predict the number of cycles to failure of a lap joint in terms of the fracture mechanics data, the material properties and the joint geometry:

$$N_f = \int_{a_o}^{a_f} \frac{\left[E_s h^3 \left[1 + e(c-a)\right]^2\right]^{n-n_2}}{D G_c^{n_2} \left[3\left[T_{\max}\left(h + t_a\right)\right]^2\right]^{n-n_1}} \cdot \left[\frac{\left[G_c E_s h^3 \left[1 + e(c-a)\right]^2\right]^{n_2} - \left[3\left[T_{\max}\left(h + t_a\right)\right]^2\right]^{n_2}}{\left[3\left[T_{\max}\left(h + t_a\right)\right]^2\right]^{n_1} - \left[G_{th} E_s h^3 \left[1 + e(c-a)\right]^2\right]^{n_1}}\right]$$

where $a_o = \frac{E_a G_c}{\pi \sigma_a^2}$

and $a_f = c - \frac{1}{e}\left[\left(\frac{3\left(T_{\max}\left[h + t_a\right]\right)^2}{E_s h^3 G_c}\right)^{1/2} - 1\right]$

7.3 DATA FITTING

The fatigue data, see Figure 5, can be split into three sections, a lower threshold section (I), where the strain energy release rate is G_{th}, a linear rising portion (II), and the upper threshold (III), G_C. Removing the threshold points leaves the rising portion, where linear regression can be used to find D and n from Equation 8 as discussed in section 5.2. The data obtained from the 'wet' tests on steel TDCB specimens bonded with 'AV119' give D and n values of 1.21 x 10^{-13} $m^2/N.cycle$, and 3.67 respectively, Table 14.

Values of n_1 and n_2 are found by substituting a high and a low experimental value of the fracture energy, with its corresponding crack growth rate, into Equation 11. This gives a pair of simultaneous equations which can be solved by iteration. The values of n_1 and n_2 are not unique, but depend on the values of G_{max} and da/dN used. However the predicted number of cycles is largely unaffected by the choice of these values. The experimental data and the model are shown in Figure 40.

The data required for the lifetime prediction model are summarised in Table 14. The adhesive properties are taken from Project 1 of the MTS Programme[25].

7.4 RESULTS

The predicted lifetime and the experimental results for the single lap joints are shown in Figure 41. In this case the agreement between the analytical and experimental results is only moderate. The fatigue life is underestimated by almost an order of magnitude. However, the predicted threshold of approximately 20 % of the static failure stress is of the correct magnitude, and lower than the 30 % observed. Thus, the prediction is a conservative one.

This method of failure prediction has been shown to fit the experimental data very well for some adhesive/substrate combinations[14,21], but poorer matches have also been found[20]. Further work will be required to identify the reasons for these differences, for example by using finite element analysis to aid the formulation of a better lap joint model.

7.5 CONCLUSIONS

A lifetime prediction model has been used to estimate the number of cycles to failure of single lap joints. This has produced conservative values of the lifetime, but requires refinement to accurately predict the full relationship between applied stress and joint lifetime. However the predicted threshold value, 20 % of the static failure stress, is close to that found experimentally.

Adhesive fracture energy	G_C, J/m^2	700
Threshold strain energy release rate	G_{th}, J/m^2	25
Modified Paris law coefficient	D, $m^2/N.cycle$	1.21×10^{-13}
Modified Paris law exponent	n	3.66
Threshold region curve fitting constant	n_1	0.519
Fast fracture region curve fitting constant	n_2	0.110
Substrate modulus	E_s, GN/m^2	210
Substrate thickness	h, mm	2.0
Adhesive modulus	E_a, GN/m^2	3.0
Adhesive Poissons ratio	υ	0.4
Adhesive fracture stress	σ_a, MN/m^2	70
Adhesive thickness	t_a, mm	0.4
Half overlap length	c, mm	6.35
Griffith flaw size (from Equation 21)	a_o, μm	135

Table 14. Values used for lap joint prediction model.

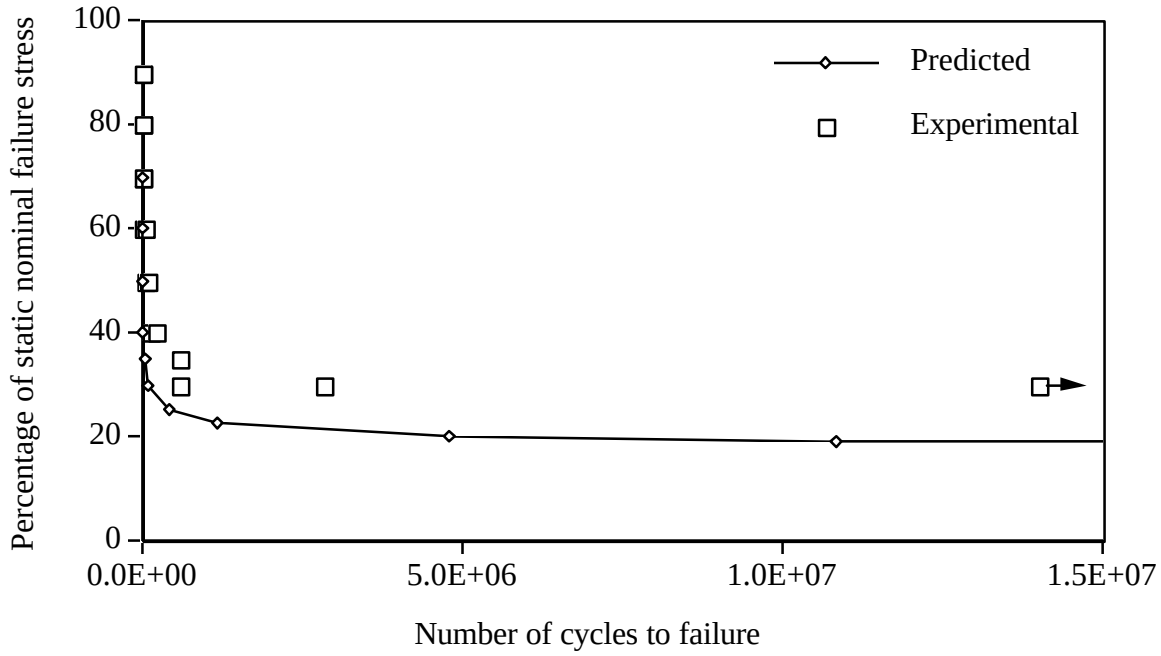

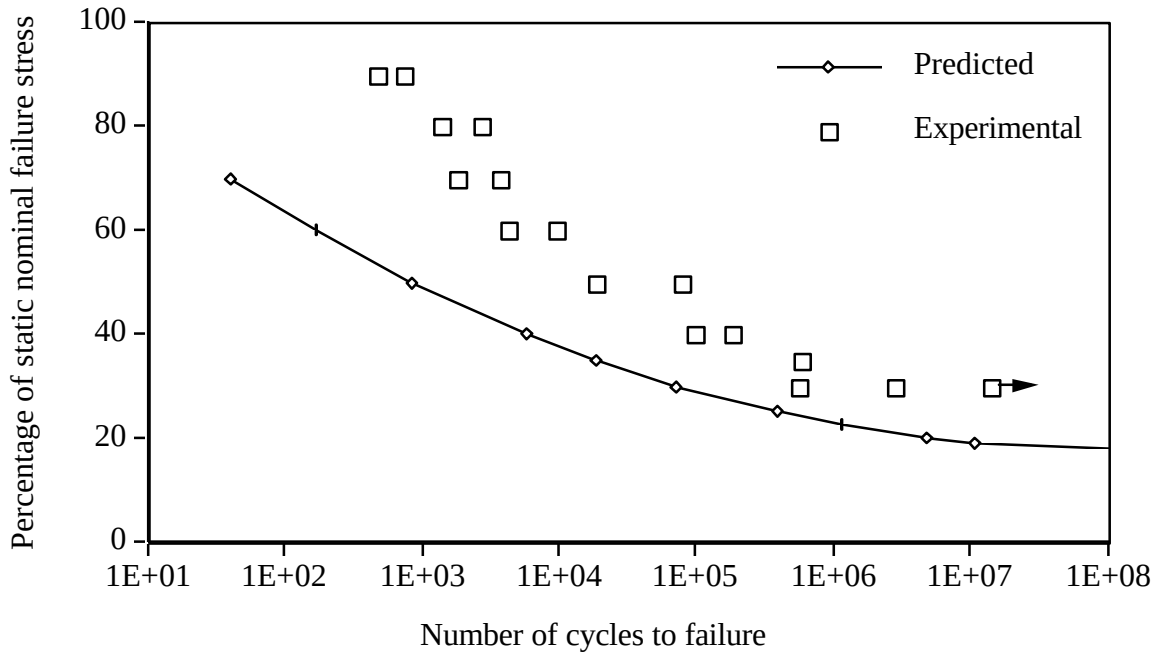

Figure 41. Predicted and experimental lifetimes for single lap joints, (a) linear axis, (b) logarithmic axis.

8 Conclusions

Static testing of bonded TDCB specimens gave G_C values of 820 J/m^2 for 'F241' and 700 J/m^2 for the 'AV119' adhesive. These were for cohesive-in-adhesive failure. Where apparently interfacial failure occurred on some 'AV119'/steel specimens, the measured fracture energy was reduced. Stick/slip failure also occured on the GB/DG aluminium and steel specimens bonded with 'AV119', and again the fracture energy was reduced.

'Wet' and 'dry' fatigue tests were conducted on TDCB specimens. All tests showed a threshold value of the fracture energy, G_{th}, below which crack growth does not occur. The value of this threshold depended on the adhesive, substrate, surface treatment and test environment. The value of the fatigue threshold, G_{th}, was far lower than the static fracture energy, G_C. For example, the 'AV119' epoxy adhesive was found to have a static G_C value of about 700 J/m^2, however in 'dry' fatigue the threshold was 170 J/m^2. Both failures were cohesive-in-adhesive. The value of G_{th} was reduced further by water immersion. For example, apparently interfacial failure occurred for the 'AV119' epoxy adhesive on a gritblasted and degreased aluminium substrate, and a value of only 25 J/m^2 was recorded. Thus, there is a 95 % reduction between the static value of G_C and the fatigue threshold, G_{th}, for a 'wet' fatigue test, using gritblasted and degreased aluminium-alloy substrates. Generally the chromic-acid etch treatment resulted in the better durability.

Steel lap joints bonded with 'AV119' were tested statically giving a nominal failure stress of 24 MN/m^2. 'Wet' fatigue tests were performed at between 30 and 90 % of the static failure stress. These showed an increasing joint life with decreasing applied stress, and produced evidence of a threshold, below which failure does not occur, at around 30 % of the static stress.

A lifetime prediction model was used to predict the fatigue life of the bonded lap joints from the TDCB fatigue data. This has produced conservative values of the lifetime, but requires refinement to predict accurately the full relationship between the cyclically applied stress and joint lifetime. However the predicted threshold value, 20 % of the static failure stress, is close to that found experimentally.

9 Acknowledgements

This work was funded by the Department of Trade and Industry Measurements, Technology & Standards programme on the performance of adhesive joints. The author wishes to thank Professor A.J. Kinloch, AEA Technology, Loughborough University, Oxford Brookes University and his colleagues at Imperial College.

10 References

1. Kinloch, A.J., Adhesion And Adhesives : Science And Technology (Chapman Hall, London, 1987).
2. Comyn, J. Kinetics and Mechanisms of Environmental Attack *in Durability of Structural Adhesives* (ed. Kinloch, A.J.) 85 - 134 (Applied Science Publishers, London & New York, 1983).
3. Water Uptake in Adhesives-Summary Report, (Oxford Brookes University, 1995).
4. Ebtahaj, K., Personal Communication, Oxford Brookes University, (1996).
5. Brockmann, W., Durability of Adhesion Between Metals and Polymers, *International Journal of Adhesion and Adhesives* **13**, 97 - 104 (1989).
6. Bull, S.J., Bellamy, B.A., Bishop, H.E., Watts, J.F. & Brewis, D., The Role of Surface Analysis in Adhesive Bonding (1995).
7. ASTM, Fracture Strength in Cleavage of Adhesives in Bonded Joints, *ASTM* **D3433**, (1975).
8. Mostovoy, S. & Ripling, E.J., Fracture Toughness of an Epoxy System, *Journal of Applied Polymer Science* **10**, 1351 - 1371 (1966).
9. Jethwa, J.K. & Kinloch, A.J. The Fatigue Performance of Adhesively Bonded Metal Joints *in Conference Proceedings of Adhesion '93* 197 - 202 (Institute of Materials, London, 1993).
10. Fernando, M., Harjoprayitno, W.W. & Kinloch, A.J., A Fracture Mechanics Study of the Influence of Moisture on the Fatigue Behaviour of Adhesively-Bonded Aluminium-Alloy Joints,
11. Williams, J.G., Fracture Mechanics of Polymers (Ellis Horwood, Chichester, 1984).
12. Martin, R.H. & Murri, G.B., Characterization of Mode I and Mode II Delamination Growth and Thresholdsin AS4/PEEK Composites, *ASTM STP* **1059**, 251 - 270 (1990).
13. Osiyemi, S.O. The Fatigue Performance of Adhesively Bonded Fibre-Composite Joints, PhD Thesis (Imperial College, University of London, 1992).
14. Jethwa, J.K. The Fatigue Performance of Adhesively-Bonded Metal Joints, PhD Thesis (Imperial College, University of London, 1995).
15. Crichlow, G., Personal Communication, Instituteof Surface Science & Technology, Loughborough, (1996).
16. Harris, J.A. & Fay, P.A., Fatigue Life Evaluation of Structural Adhesives for Automotive Applications, *International Journal of Adhesion and Adhesives* **12**, 9 - 18 (1992).
17. ASTM, Strength Properties of Adhesives in Shear by Tension Loading (Metal-to-Metal), *ASTM* **D1002**, (1983).
18. Zhang, Z., Shang, J.K. & Lawrence, F.V., A Backface Strain Technique for Detecting Fatigue Crack Initiation in Adhesive Joints, *Journal of Adhesion* **49**, 23 - 36 (1995).
19. Imanaka, M., Haraga, K. & Nishikawa, T., Fatigue Strength of Adhesive/Rivet Combined Lap Joints, *Journal of Adhesion* **49**, 197 - 209 (1995).
20. Fernando, M. & Dyson, I.G., Personal Communication, Imperial College of Science, Technology and Medicine, (1996)
21. Kinloch, A.J. & Osiyemi, S.O., Predicting the Fatigue Life of Adhesively-Bonded Joints, *Journal of Adhesion* **43**, 79 - 90 (1993).
22. Hart-Smith, L.J., Designing to Minimize Peel Stresses in Adhesive-Bonded Joints, *ASTM STP* **876**, 238 - 266 (1985).

23. Zhao, X., Adams, R.D. & Pavier, M.J. A New Approach to Determining the Bending Moment Factors in Single Lap Joints, 1-35/1 - 35/6 (Plastics and Rubber Institute, Cambridge, UK, 1990).
24. Williams, J.G., On the Calculation of Energy Release Rates for Cracked Laminates, *International Journal of Fracture* **36**, 101 - 119 (1988).
25. Minutes of Meeting, (MTS Programme Industrial Advisory Group, 1995).